



RESEARCH ARTICLE

Comparative localization of colorectal sensory afferent central projections in the mouse spinal cord dorsal horn and caudal medulla dorsal vagal complex

QingQing Wang^{1,2} | Sonia Garcia Caraballo^{1,2} | Grigori Rychkov^{2,4}  |
 Alice E. McGovern³ | Stuart B. Mazzone³ | Stuart M. Brierley^{1,2,4} |
 Andrea M. Harrington^{1,2,4} 

¹Visceral Pain Research Group, College of Medicine and Public Health, Flinders Health and Medical Research Institute, Flinders University, Adelaide, South Australia, Australia

²Hopwood Centre for Neurobiology, Lifelong Health, South Australian Health and Medical Research Institute (SAHMRI), Adelaide, South Australia, Australia

³Department of Anatomy and Physiology, The University of Melbourne, Melbourne, Victoria, Australia

⁴School of Biomedicine, Faculty of Health and Medical Sciences, University of Adelaide, Adelaide, South Australia, Australia

Correspondence

Andrea M. Harrington, Visceral Pain Research Group, Level 7, South Australia Health and Medical Research Institute, North Terrace, Adelaide, South Australia 5000, Australia.
 Email: andrea.harrington@flinders.edu.au

Parts of this work have appeared in presentations at the Australasian Neuroscience Society annual meeting 2019 and Society for Neuroscience: Global Connectome Virtual Conference 2021.

Funding information

Australian Research Council, Grant/Award Number: DP180101395; National Health and Medical Research Council of Australia (NHMRC), Grant/Award Number: APP2008727

Abstract

The distal colon and rectum (colorectum) are innervated by spinal and vagal afferent pathways. The central circuits into which vagal and spinal afferents relay colorectal nociceptive information remain to be comparatively assessed. To address this, regional colorectal retrograde tracing and colorectal distension (CRD)-evoked neuronal activation were used to compare the circuits within the dorsal vagal complex (DVC) and dorsal horn (thoracolumbar [TL] and lumbosacral [LS] spinal levels) into which vagal and spinal colorectal afferents project. Vagal afferent projections were observed in the nucleus tractus solitarius (NTS), area postrema (AP), and dorsal motor nucleus of the vagus (DMV), labeled from the rostral colorectum. In the NTS, projections were opposed to catecholamine and pontine parabrachial nuclei (PbN)-projecting neurons. Spinal afferent projections were labeled from rostral through to caudal aspects of the colorectum. In the dorsal horn, the number of neurons activated by CRD was linked to pressure intensity, unlike in the DVC. In the NTS, 13% ± 0.6% of CRD-activated neurons projected to the PbN. In the dorsal horn, at the TL spinal level, afferent input was associated with PbN-projecting neurons in lamina I (LI), with 63% ± 3.15% of CRD-activated neurons in LI projecting to the PbN. On the other hand, at the LS spinal level, only 18% ± 0.6% of CRD-activated neurons in LI projected to the PbN. The collective data identify differences in the central neuroanatomy that support the disparate roles of vagal and spinal afferent signaling in the facilitation and modulation of colorectal nociceptive responses.

KEYWORDS

colorectal distension, gut–brain axis, neuroanatomy and spinal cord dorsal horn, spinal afferent, vagal afferent, visceral pain

Abbreviations: AP, area postrema; DGC, dorsal gray commissure; DMV, dorsal motor nucleus of the vagus; LI, lamina I; LV, lamina V; NTS, nucleus of the solitary tract; SPN, sacral parasympathetic nucleus.

This is an open access article under the terms of the [Creative Commons Attribution](https://creativecommons.org/licenses/by/4.0/) License, which permits use, distribution and reproduction in any medium, provided the original work is properly cited.

© 2023 The Authors. *The Journal of Comparative Neurology* published by Wiley Periodicals LLC.

1 | INTRODUCTION

Distension of the colon and rectum (colorectum) stimulates affective visceromotor reflexes associated with sensations of the urge to defecate and discomfort (Harrington et al., 2018). Colorectal distension (CRD) at innocuous pressures (15–30 mmHg), which are pertinent to stool passage, evokes minimal visceromotor responses (i.e., below level of sensation) but stimulates autonomic motor reflexes to support defecation (Christianson et al., 2007; Grundy et al., 2018). In contrast, noxious pressures of CRD (40–80 mmHg), which are relevant to discomfort, evokes significant visceromotor responses that engage both nociceptive and defecatory motor responses (Christianson et al., 2007; Grundy et al., 2018). Regulating colorectal visceromotor responses, such that they are proportionate to stimulus intensity, involves the sensory neurons innervating the colorectum that relay into the central nervous system via the spinal (lumbar splanchnic and sacral pelvic nerve) and vagal (celiac and accessory celiac branches of the vagus nerve) afferent pathways (Harrington et al., 2018). Functional studies show that CRD-evoked nociceptive responses are attenuated by blocking spinal afferent signaling (Kyloh et al., 2022; Ness, 2000; Palecek et al., 2003; Zhang et al., 2011), while, conversely, they are enhanced by vagotomy (Chen et al., 2008; Gschossman et al., 2002). Such disparity may reflect differences between the central circuits into which spinal and vagal pathways relay colorectal nociceptive information. However, to date, comparative assessments of the vagal and spinal afferent innervation of the colorectum have focused on peripheral properties, such as the abundance, sensitivity, and location of endings within the colon wall (Herrity et al., 2014; Meerschaert et al., 2020; Osman et al., 2023; Robinson et al., 2004; Wang et al., 2000). Thus, there is a paucity of information on the central anatomy of vagal and spinal colorectal afferent pathways to establish if they may differently engage central circuits involved in pain facilitation and modulation.

From retrograde studies in rats, we know that vagal afferents innervating the caecum through to the distal colon, but not the rectum, project into the nucleus of the solitary tract (nucleus tractus solitarius [NTS]) within the caudal medulla dorsal vagal complex (DVC) (Altschuler et al., 1991, 1993). Beyond this information, there is scant knowledge of the DVC circuits into which vagal afferents relay colorectal information to elucidate how they may mediate an antinociceptive influence on colorectal nociceptive responses (Wang et al., 2009). As for the spinal innervation, retrograde tracing studies, in both rats and mice, illustrate that the spinal afferent innervation of the distal colon through to the rectum projects into discreet regions of the dorsal horn within the thoracolumbar (TL; T10–L1) and lumbosacral (LS; L5–S2) spinal cord (Ge et al., 2019; Harrington et al., 2019). In contrast to the vagal pathway, numerous studies have explored various aspects of the dorsal horn circuits processing colorectal afferent input (Harrington, 2023). Collectively, these studies indicate that the dorsal horn circuits facilitating colorectal nociceptive transmission into the brain differ between the TL and LS spinal cord (Harrington et al.,

2019; Katter et al., 1996; Murphy et al., 2009; Ness et al., 1987, 1988, 1989; Palecek & Willis, 2003; Palecek et al., 2003; Traub et al., 1993, 2002; Wang et al., 2005). However, the spatial relationship between colorectal spinal afferent input and specific dorsal horn nociceptive circuits remains to be assessed between the TL and LS dorsal horn. Somatosensory nociceptive ascending relay involves TRPV1-positive afferent terminals directly recruiting dorsal horn lamina I (LI) neurons projecting to the pontine lateral parabrachial nuclei (PbN) (Cameron et al., 2015; Hwang et al., 2003; Wercberger et al., 2019). It is unknown if colorectal afferents, moreover viscerosensory afferents in general, have a comparable relationship to PbN-projection neurons within the dorsal horn LI.

To address these knowledge gaps, this study aimed to compare the central anatomy of the vagal and spinal afferent pathways innervating different regions of the mouse colorectum—specifically, by localizing where vagal and spinal colorectal afferents project within DVC and dorsal horn, and correlating this input to the degree and distribution of neuronal activation evoked by CRD (at innocuous and noxious pressures) within circuits involved in nociceptive and sensory–motor integration.

2 | MATERIALS AND METHODS

2.1 | Animals

Female and male C57BL/6J (8–16 weeks, weight range 18–30 g) mice were used, with specific numbers for individual data sets noted in figure legends. All experiments were performed in accordance with the approval of Animal Ethics Committees of the South Australian Health and Medical Research Institute (SAHMRI; Application SAM190). Mice were sourced from the SAHMRI in-house breeding colony (rederived from JAX strain #000664; originally purchased from The Jackson Laboratory; breeding barn MP14) bred and housed in a specific and opportunistic pathogen-free facility. Mice were group housed (five mice per cage) prior to surgical approaches and then individually housed within ventilated cages (IVC), filled with dust-free coarse chip aspen bedding (Catalogue #: ASPJMAEBCA; PuraBed). Cages were stored on IVC racks within a temperature-controlled environment of 22°C and a 12-h light/12-h dark cycle. Mice had free access to LabDiet JL Rat and Mouse/Auto6F chow (Catalogue #: 5K52) and autoclaved reverse osmosis water.

2.2 | Cholera toxin subunit B retrograde tracing from the colorectum

Retrograde tracing using cholera toxin subunit B (CTB, 0.5%) directly conjugated to AlexaFluor AF594, AF488, or AF647 (CTB-594, Catalogue #: C22842; CTB-488, Catalogue #: C22841; CTB-647, Catalogue #: C34778; Invitrogen, ThermoFisher Scientific) was performed from

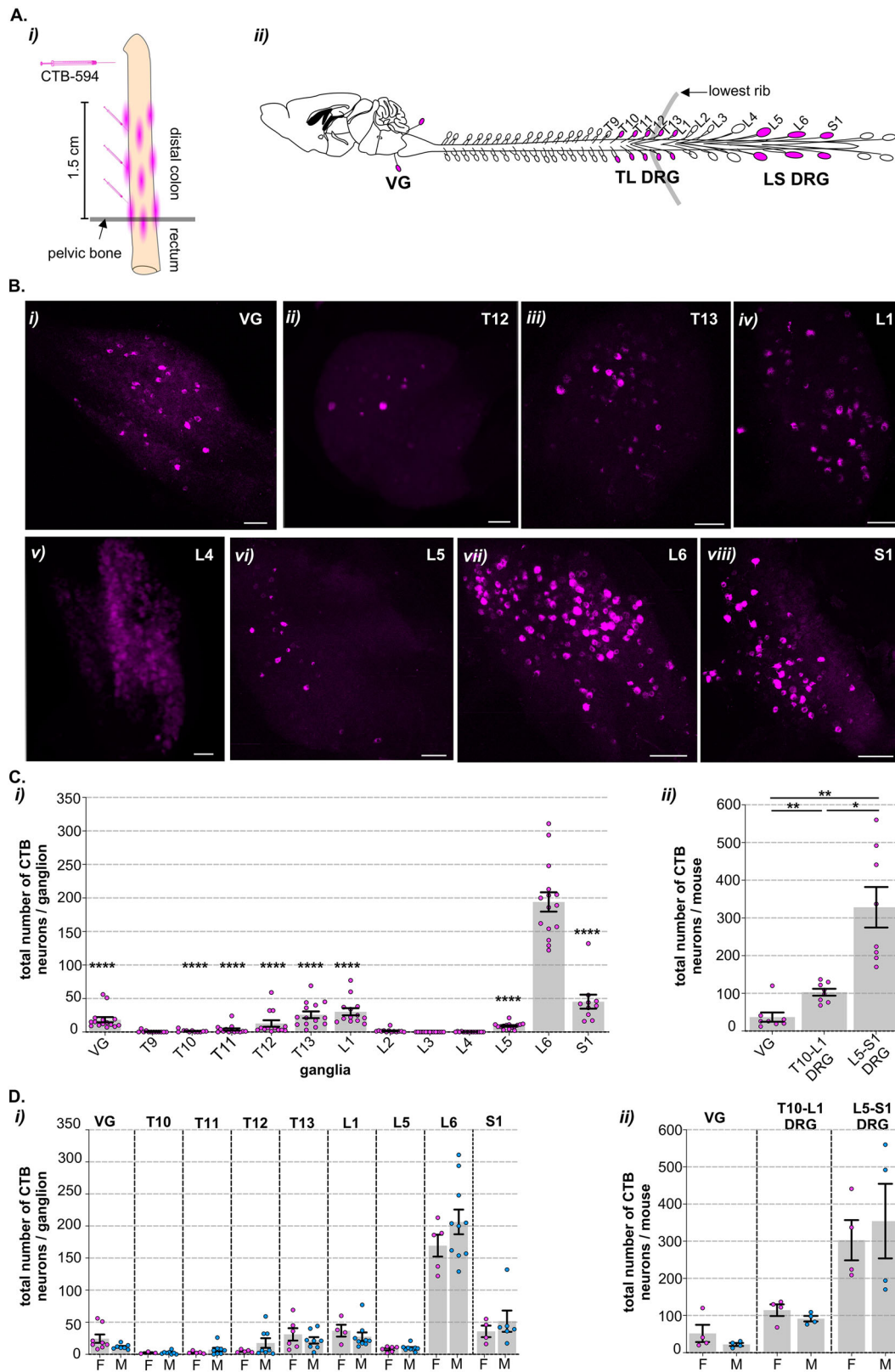


FIGURE 1 Comparative abundance of afferent neurons retrogradely labeled from the colorectum in whole vagal nodose/jugular ganglia (VG) and spinal dorsal root ganglia (DRG). (A) (i) Schematic showing the sites of retrograde tracer CTB-AF (CTB-594; magenta) injections at multiple sites of the colorectum (0.5 cm below the pelvic bone through to 1.5 cm proximal to the pelvic bone). (ii) Schematic showing the location of vagal nodose/jugular ganglia (VG) and dorsal root ganglia (DRG) collected at spinal levels thoracic 9 through to 13 (T9–T13), lumbar 1 through to 6 (L1–L6), and sacral 1 (S1). Ganglia in which colorectal retrograde-labeled neurons were observed are highlighted in magenta. (B) Representative

(Continues)

FIGURE 1 (Continued)

photomicrographs of CLARITY-cleared whole (i) VG and DRG at (ii) T12, (iii) T13, (iv) L1, (v) L4, (vi) L5, (vii) L6, and (viii) S1, 4 days after multiple injections of CTB-594 into the colorectal wall. Scale bars = 100 μ m. Photomicrographs are maximum z-projection reconstructions from confocal-collected 10–30 optical sections (10- μ m-thick z-steps). (C) Quantification of the number of (i) CTB-594-labeled neurons within individual whole VG and DRG (T9 through to S1) and (ii) CTB-594-labeled neurons in ganglia grouped within their corresponding primary afferent pathway, vagal (VG), splanchnic (T10–L1 DRG), and pelvic (L5–S1 DRG). (i) Individual data points represent the total number of CTB-594-labeled neurons within individual ganglia, with $n = 10–15$ ganglia/level. The error bars represent the standard error of the mean. **** $p < .0001$ indicates relative to L6 DRG determined by a Brown–Forsythe and Welch ANOVA test (standard deviations significantly differ between groups, mixed parametric/nonparametric data) with Dunnett’s T3 multiple comparison tests. (ii) Individual data points represent the total number of CTB-594-labeled neurons within ganglia pooled to afferent pathway per mouse, $N = 8$ (4 female, 4 male), and error bars represent the standard error of the mean. * $p < .05$ and ** $p < .01$, determined by Brown–Forsythe and Welch ANOVA test (standard deviations significantly differ between groups, mixed parametric/nonparametric data) with Dunnett’s T3 multiple comparison tests. (D) The number of CTB-594-labeled neurons within (i) individual VG and DRG (T10–L1 and L5–S1) or (ii) ganglia grouped within their corresponding primary afferent pathway, vagal (VG), splanchnic (T10–L1 DRG), and pelvic (L5–S1 DRG) did not significantly differ between female (F; pink dots) and male (M; blue dots) mice. Statistical tests used (i) Brown–Forsythe and Welch ANOVA test with Dunnett’s T3 multiple comparison tests and (ii) one-way ANOVA (parametric data) with Bonferroni multiple comparison tests. $n = 4–10$ ganglia/level; $N = 4$ female and $N = 4$ male. Error bars represent the standard error of the mean.

circumferential locations (midline, left, and right) of the colorectal wall (Harrington et al., 2019). A small aseptic abdominal incision was made in mice anesthetized with isoflurane (2%–4% in oxygen). The colorectum was located and injections were made into the wall of the colorectum that covered 0.5 cm distal and 1.5 cm proximal to the pelvic bone. CTB-AF594 was injected at three to four sites (2 μ L/injection) into the wall at circumferential left, circumferential right, and midline locations (Figure 1Ai). For regional mapping from this length of colorectum (Figure 2Ai), two 2- μ L injections of CTB-488 were made at and just caudal to the pelvic bone (caudal injections), two 2- μ L injections of CTB-594 were made between 0.5 and 1 cm proximal to the pelvic bone (intermediate injections), and two 2- μ L injections of CTB-647 were injected at 1.5 cm proximal to the pelvic bone (rostral injections). Injections were made with a 30-gauge needle (HAMC7803-07, point style: 4 [10–12°]; Hamilton Company, Bio-Strategy) attached to Hamilton 5- μ L syringe (HAMC7634-01 5 μ L 700 series RN syringe; Hamilton Company, Bio-Strategy). The needle tip was inserted into the subserosal wall space and tunneled a short distance caudally, ensuring the needle tip was always visible through the serosa and care was taken not to insert the tip into the lumen. The dye was expelled as the needle was gradually pulled out of the needle track. Suitable injections within the wall were indicated by the formation of dye boluses that were contained within the wall space. The abdominal incision was then sutured closed; analgesic (buprenorphine, 0.1 mg/kg) and antibiotic (ampicillin, 50 mg/kg) administration were given subcutaneously as mice regained consciousness. Mice were then allowed to recover, housed individually, and closely monitored. To assess labeling of colorectal afferent neurons in sensory ganglia, mice underwent transcardial perfuse fixation 4 days after retrograde tracing. To identify afferent projections in the spinal cord and medulla, mice underwent transcardial perfuse fixation 7 days after retrograde tracing.

2.2.1 | Transcardial perfuse fixation and CLARITY clearing of sensory ganglia

Mice were euthanized with an overdose of Lethobarb (60 mg/kg pentobarbitone sodium solution; Virbac Australia), via intraperitoneal injection, prior to opening the chest cavity and injecting 0.5 mL of heparin saline into the left ventricle, and insertion of a 22-gauge needle, attached to tubing and a peristaltic perfusion pump, into the left ventricle. The right atrium was then snipped allowing for perfusate drainage. Warm saline (0.85% physiological sterile saline) was perfused prior to ice-cold 4% paraformaldehyde (PFA) in 0.1 M phosphate buffer (Sigma–Aldrich). Following complete perfusion, left and right vagal ganglia (VG; fused nodose and jugular ganglia) and dorsal root ganglia (DRG; T8–S1) were removed, with the lowest rib used as an anatomical landmark for T13 DRG. Ganglia were then subjected to CLARITY clearing to remove lipids and render ganglia transparent (Grundy et al., 2018). Ganglia were kept in 4% PFA-hydrogel solution (4% acrylamide, 0.25% VA-044 in phosphate-buffered saline [PBS]) at 4°C for a minimum of 24 h. Residual oxygen was removed from samples, using a standard vacuum pump and desiccation chamber attached to a nitrogen gas supply (Tomer et al., 2014). Samples were degassed in their tubes for 10 min before being transferred to a 37°C water bath for 2 h until hydrogel solution had uniformly polymerized (Tomer et al., 2014). Tissue was removed from the hydrogel and subjected to passive clearing in 8% SDS/200 mM boric acid buffer in a gentle shaking water bath (37°C). Buffer was changed every 3 days until samples were transparent, at which point they were washed with PBS before placing individual ganglion into an 18-well glass slide. One hour prior to confocal microscopy, RapiClear 1.47 refractive index solution (SunJin Lab) was applied to wells prior to placement of a glass coverslip.

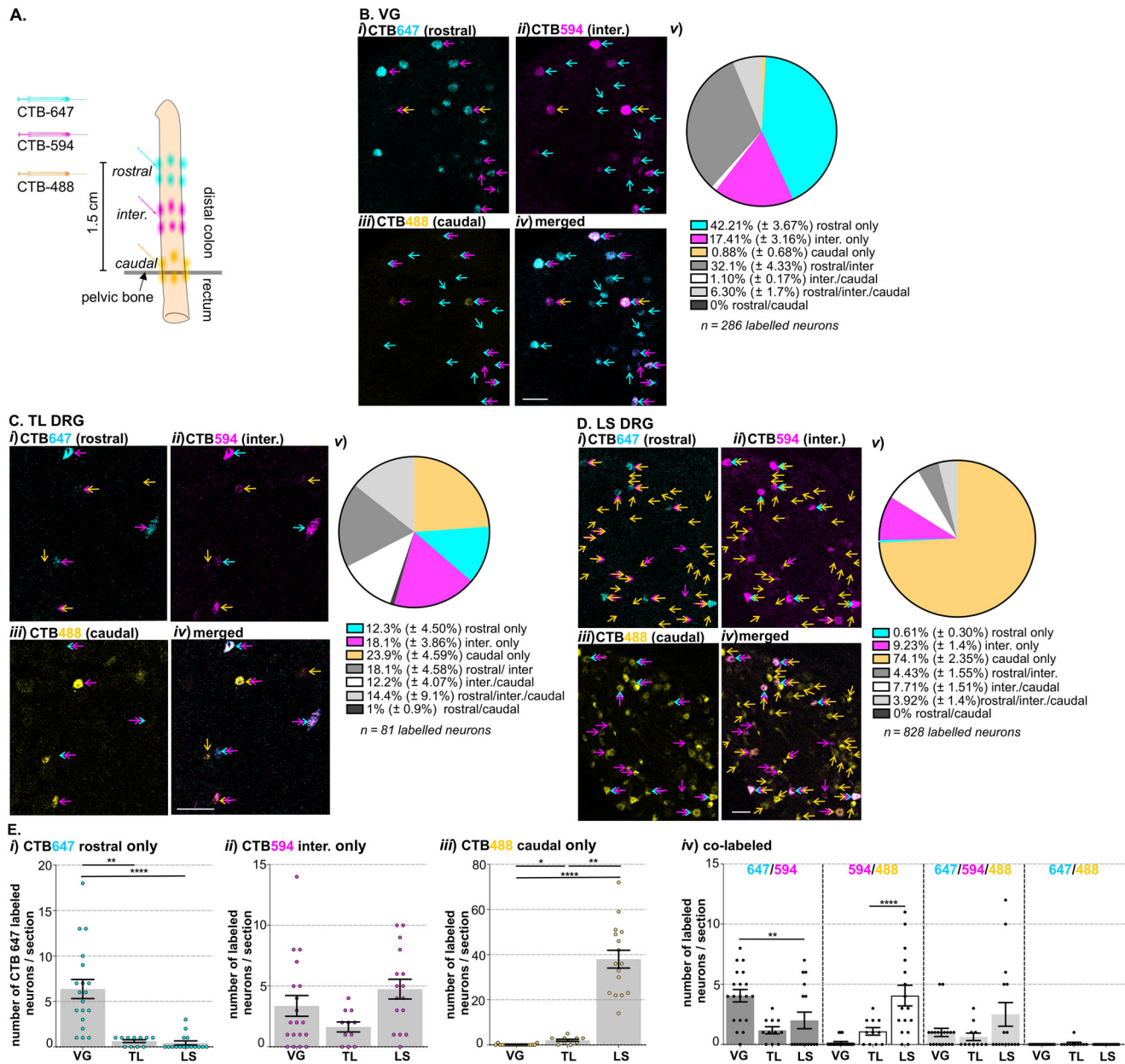


FIGURE 2 Comparative abundance of neurons labeled from regional colorectal retrograde tracing in the vagal nodose/jugular ganglia (VG) and dorsal root ganglia (DRG). (A) Schematic showing the sites of retrograde tracer injections in different regions of the colorectum. CTB-647 (cyan) was injected into the most rostral portion of the distal colon (1.5 cm proximal to the pelvic bone), CTB-594 (magenta) was injected into the intermediate (inter.) portion (covering 0.5–1 cm proximal to the pelvic bone), and CTB-488 (yellow) was injected into the most caudal portion of the distal colon and rectum (injections at and below the pelvic bone). Representative photomicrographs of (B) nodose/jugular ganglia (VG), (C) thoracolumbar (TL), and (D) lumbosacral (LS) DRG sections showing (i) CTB-647 (cyan), (ii) CTB-594 (magenta), (iii) CTB-488 (yellow) neurons, and (iv) co-labeled neurons (white) and their (v) relative proportions (percentage \pm standard error of the mean) of the total number of labeled neurons following rostral, intermediate (inter.), and caudal-directed colorectal CTB injections. Labeled neurons are highlighted with colored arrows: cyan = rostral CTB-647, magenta = inter. CTB-594, and yellow = caudal CTB-488. Multiple headed arrows indicate neurons labeled from multiple injection sites. Scale bars = 100 μ m. (E) Quantification of the total number of (i) CTB-647, (ii) CTB-594, (iii) CTB-488, and (iv) co-labeled neurons within sections of VG, TL DRG, and LS DRG. Individual data points represent the number of CTB-labeled neurons within individual sections and error bars represent the standard error of the mean. * $p < .05$, ** $p < .01$, and **** $p < .0001$, determined by a Kruskal–Wallis ANOVA test (nonparametric) with Dunn’s multiple comparison tests. Data are from $N = 4$ male mice, 3–5 sections/ganglia.

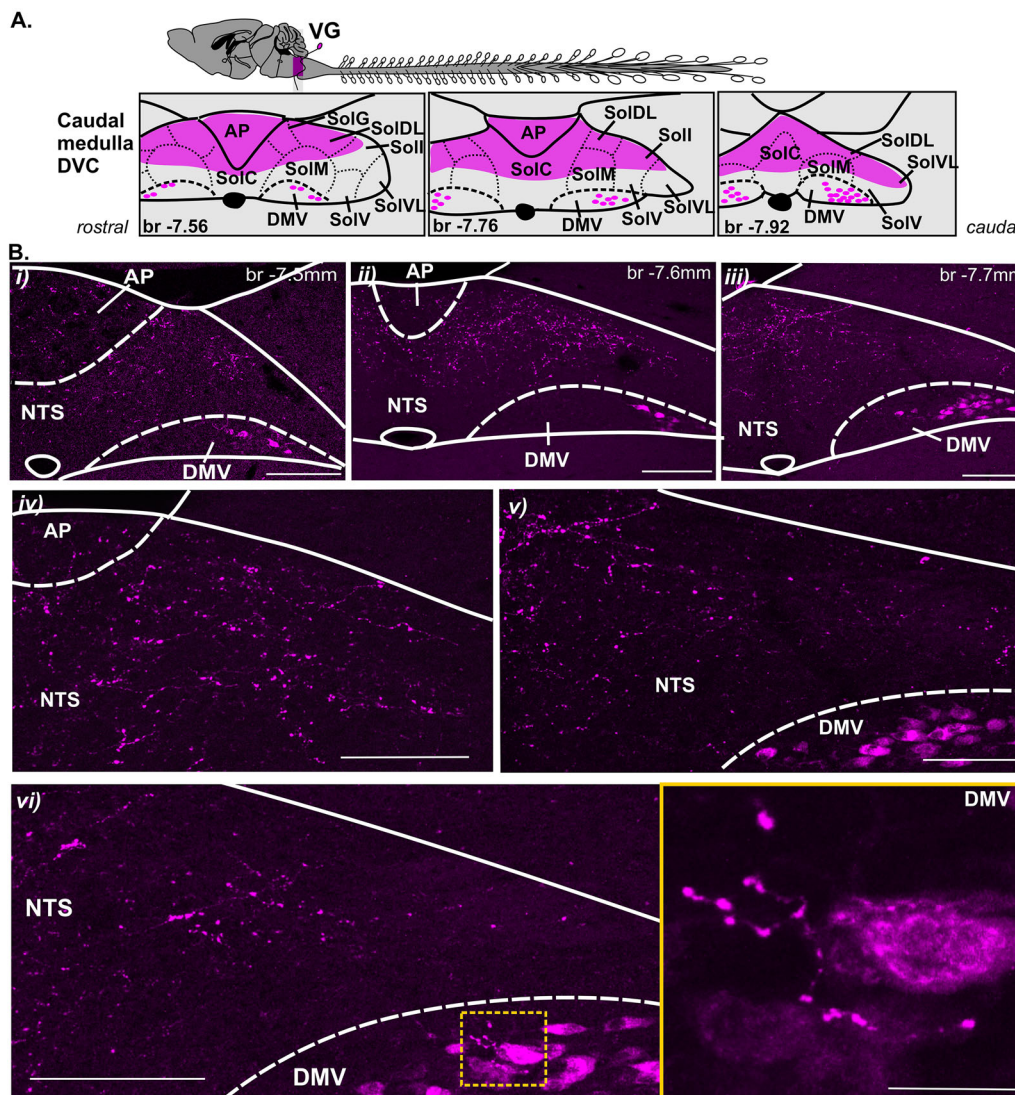


FIGURE 3 Distribution of colorectal retrograde-labeled fibers and cell bodies within the dorsal vagal complex (DVC) of the caudal medulla. (A) Schematic illustration of the caudal medulla DVC at distances from bregma (br) based on Paxinos et al. (2001) showing the distribution of labeled fibers and cell bodies (indicated by magenta shaded areas) following colorectal retrograde tracing. Observational data gained from $N = 8$ mice (4 female, 4 male). (B) Representative photomicrographs of the DVC at (i–iii) low magnification and (iv–vi) high magnification showing the distribution of colorectal-labeled fibers and cell bodies (magenta) at the (i) rostral, (ii) intermediate, and (iii, v, and vi) caudal aspects of the caudal medulla. Rostral–caudal aspect based on approximate distance from bregma (br) (Paxinos et al., 2001). (vi) Image in the yellow-lined box (scale = $20\ \mu\text{m}$) is a higher magnification image of the region within the yellow-dotted box. Scale bars: i–iv = $100\ \mu\text{m}$; v and vi = $50\ \mu\text{m}$. Photomicrographs are maximum z-projections from nine to 10 confocal optical sections. AP, area postrema; DMV, dorsal motor nucleus of the vagus; NTS, nucleus of the solitary; SolC, nucleus of the solitary tract commissural; SolDL, nucleus of the solitary tract dorsolateral; SolG, nucleus of the solitary tract gelatinous; Soll, nucleus of the solitary tract interstitial; SolM, nucleus of the solitary tract medial; SolV, nucleus of the solitary tract ventral; SolVL, nucleus of the solitary tract ventrolateral.

2.2.2 | Stereotaxic surgery and retrograde tracing from the lateral PbN

Mice were anesthetized with isoflurane and administered analgesia (buprenorphine) via subcutaneous injection, before being placed in a stereotaxic frame (MTM-3; WPI Ltd.). Under continual delivery of isoflurane, via a nose cone mask, an incision was made through the scalp and the skull was exposed. A burr hole was made through the skull, and a single unilateral injection of 300 nL (40 nL/min) of 0.5%

CTB-594 was made targeting the left PbN. Injections were made using a 34-gauge needle (HAMC207434 point style: 4 [10–12°]; Hamilton Company, Bio-Strategy) attached to a $2.5\text{-}\mu\text{L}$ Hamilton syringe (HAMC7632-01,62 RN; Hamilton Company, Bio-Strategy) controlled by a microinjector syringe pump (UMP3T-1; WPI Ltd.) and using the following coordinates: -4.9 to -5 mm posterior to Bregma, -1.4 mm lateral from midline, and -2.90 mm ventral to dura. The needle was left in place for 5 min after the injection was completed to minimize leakage of tracer. After slow withdrawal of the needle and suture closure of

TABLE 1 Details of primary and secondary antibodies used.

A) Primary antibodies						
Antigen	Species raised in	Manufacturer code	Manufacturer	Dilution	RRID	
Choline acetyltransferase (ChAT)	Goat	AB144P	SIGMA (Millipore)	1:100	AB_2079751	
Calcitonin gene-related peptide (CGRP)	Rabbit	PC205L	Millipore	1:200	AB_564312	
Phospho-p44/42 MAPK (Erk1/2) (Thr202/Tyr204) (D13.14.4E) XP(tm) mAb (pERK)	Rabbit	4370	Cell Signaling	1:100 (immunofluorescence detection) 1:800 (DAB detection)	AB_2315112	
Tyrosine hydroxylase (Isotype IgG1)	Mouse	22941	ImmunoStar	1:1000	AB_572268	
B) Secondary antibodies						
Antigen	Species raised in	Conjugate	Manufacturer code	Manufacturer	Dilution	RRID
Rabbit IgG H+L	Chicken	488	A21441	ThermoFisher	1:200	AB_2535859
Rabbit IgG H+L	Chicken	647	A21443	ThermoFisher	1:200	AB_2535861
Mouse IgG1	Goat	647	A21240	ThermoFisher	1:200	AB_2535809
Goat IgG H+L	Chicken	647	A21469	ThermoFisher	1:200	AB_10374877

the scalp incision, mice were removed from the frame and either placed in a clean cage and monitored for 2–4 h postrecovery or immediately subjected to a laparotomy for retrograde tracing of the colorectum (using CTB-488) as described above. After a 7-day survival period, mice that underwent PbN and colorectal tracing were transcardial perfuse fixed as outlined above. Mice that underwent PbN tracing, but not colorectal tracing, were subjected to noxious *in vivo* CRD as outlined below. Injections sites were verified in brainstem sections and mice with CTB fluorescence localized to the PbN, inclusive of the lateral and medial parabrachial area and Kölliker–Fuse nucleus, were used for subsequent quantification (Cameron et al., 2015; Tokita et al., 2009). Only male mice were used given that previous studies in rats show that PbN-projecting neurons are more responsive to noxious CRD in males relative to females (Murphy et al., 2009).

2.3 | *In vivo* CRD

Following isoflurane anesthesia, mice were given an enema of sterile saline followed by insertion of a 2-cm balloon catheter into the perianal canal. When the base of the balloon was localized approximately 0.2 cm from the anal verge, the catheter tube was secured in place by taping it to the base of the tail (Christianson et al., 2007). Mice were then placed in a Perspex box, and the balloon catheter was distended to 80 mmHg (noxious) of pressure applied via a syringe attached to three-way valve and monitored via a sphygmomanometer. Distension was held for 10 s, then released for 5 s. This sequence was repeated five times (Castro et al., 2013, 2017; de Araujo et al., 2014; Grundy et al., 2018; Harrington et al., 2012, 2019). A separate cohort of mice were

subjected to balloon insertion without distension (no CRD) or distension to 20 mmHg (nonnoxious CRD) (Brierley et al., 2004; Harrington et al., 2019). Immediately after the fifth distension, mice were placed into an isoflurane induction chamber, and within 30–40 s, they were administered an overdose of euthanasia agent (Lethobarb via intraperitoneal injection) and subjected to transcardial perfusion fixation as outlined above. Fixation was completed within 5–6 min after the final distension.

2.4 | Tissue processing of sensory ganglia, spinal cord, and medulla samples for cryosectioning

Following complete perfuse fixation (as described above), sensory ganglia (VG and DRG [T10–L1 and L5–S1]), spinal cord, and brain were collected and postfixed in 4% PFA in 0.1 M phosphate buffer at 4°C for 18–20 h prior to cryoprotection in 30% sucrose/phosphate buffer (Sigma–Aldrich) overnight at 4°C (Harrington et al., 2019). Ganglia were then placed in 100% OCT (Tissue-Tek O.C.T. Compound; Sakura Finetek) and snap frozen in liquid nitrogen. The spinal cord and brain were subjected to an additional 24-h incubation at 4°C in 50% OCT/30% sucrose/phosphate buffer solution before freezing in 100% OCT. Tissue was cryosectioned and cross sections were placed onto gelatin-coated slides to visualize CTB-AF (20- to 50- μ m thick) or immunolabeling (10- μ m thick). For the TL spinal cord, sequential sections (20–50 μ m) spanning the entire T10–T12 and T13–L1 segments collected were visualized for CTB-AF. For LS spinal cord, the spinal cord removed from below vertebrae L2 was sectioned in its entirety beginning from the top (which is equivalent to spinal cord level L5).

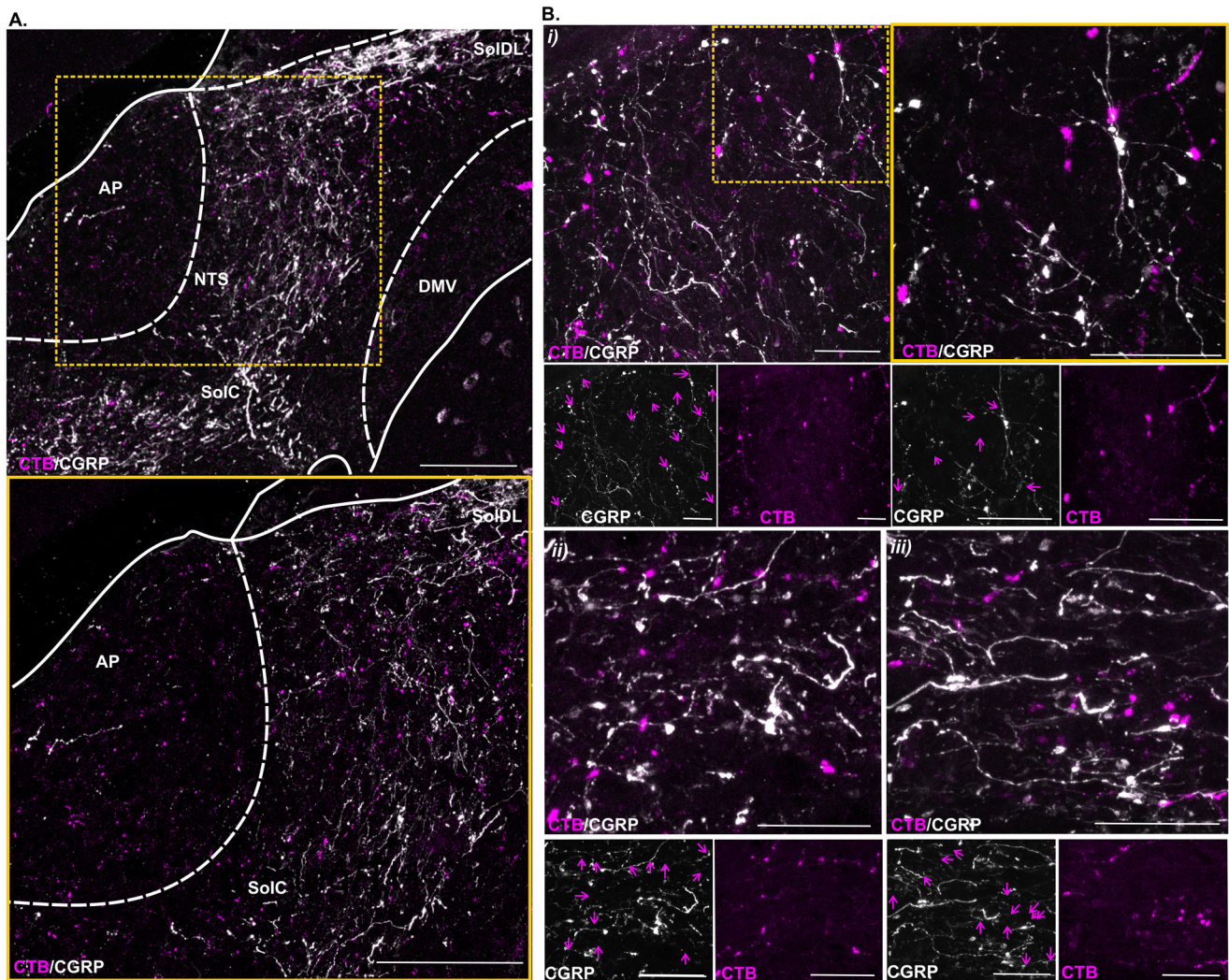


FIGURE 4 Distribution of colorectal retrograde-labeled fibers in the DVC relative to calcitonin gene-related peptide-immunoreactive fibers (CGRP-IR). (A) Low-magnification photomicrographs of the DVC showing the distribution of colorectal-labeled fibers (CTB-594, magenta) in the nucleus of the solitary tract (NTS) and area postrema (AP) relative to the distribution of fibers immunoreactive for calcitonin gene-related peptide (CGRP; gray). Yellow-bordered image corresponds to the region within the yellow-dotted box. Scale bars = 100 μm . SolC, nucleus of the solitary tract commissural; SolDL, nucleus of the solitary tract dorsolateral. (B) (i–iii) High-magnification photomicrographs showing colorectal-labeled fibers (CTB-594, magenta) in relation to CGRP-IR fibers (gray) in the NTS. Colorectal-labeled fibers are indicated by magenta arrows in CGRP-only figure panels. (i) Yellow-bordered image corresponds to the region within the yellow-dotted box. Photomicrographs are maximum z-projections from three to four confocal optical sections (2- μm -thick z-steps). Scale bars = 20 μm .

Sections were routinely visualized under a fluorescent microscope during cryosectioning to identify when CTB-AF-labeled projections appeared and disappeared. The L5–S1 spinal cord segments were subsequently identified *ex vivo* based on shape of dorsal horn and the presence or absence of sacral parasympathetic nuclei (SPNs) using the Allen Institute Mouse Spinal Cord Atlas (<https://mousespinal.brain-map.org/imageseries/showref.html>) (Lein et al., 2007). The medulla was sectioned in a similar fashion, with the caudal medulla identified by the presence and shape of the area postrema (AP) in reference

to the Paxinos and Franklin Mouse Brain Atlas (Paxinos et al., 2001). Sections were then dried on slides for an hour and washed in 0.2% Triton-X 100 (Sigma–Aldrich) in 0.1 M phosphate-buffered saline (T-PBS) before cover slipping with ProLong Diamond Antifade Mountant with DAPI (P36966; Invitrogen, ThermoFisher Scientific) and air dried for 24 h prior to microscopy. Ganglia, spinal cord, and medulla sections (10 μm) were also collected and distributed over slides (sections 50–200 μm apart) and processed for immunolabeling as outlined below.

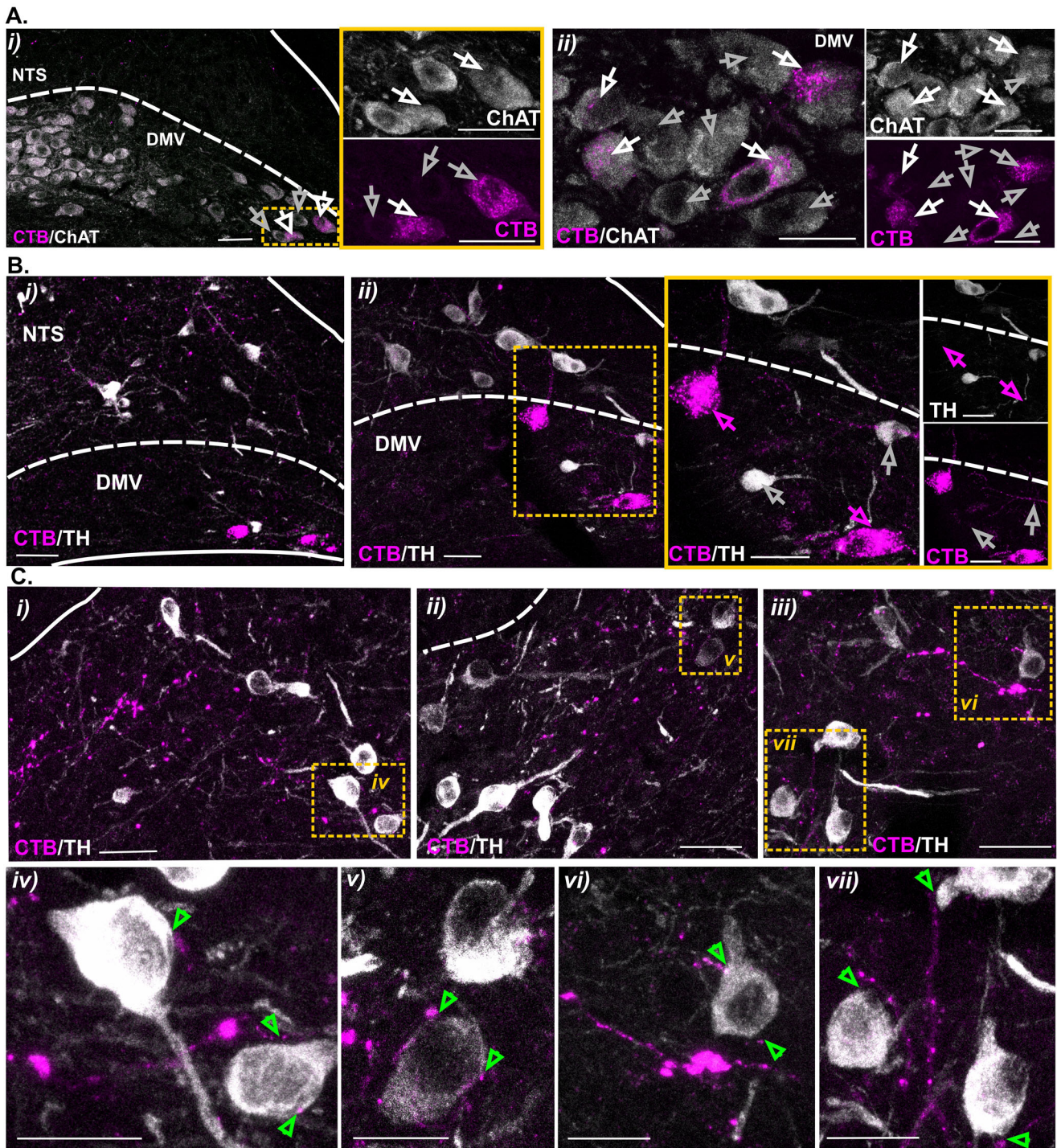


FIGURE 5 Colorectal retrograde-labeled neurons in the dorsal motor nucleus of vagus (DMV) labeled for choline acetyltransferase (ChAT) but not tyrosine hydroxylase (TH). (A, B) Photomicrographs of colorectal-labeled cell bodies (CTB, magenta) in the DMV immunolabeled for (Ai–ii) choline acetyltransferase (ChAT, gray) but not (Bi–ii) tyrosine hydroxylase (TH, gray). Co-labeled neurons are indicated by white arrows, colorectal-labeled neurons are indicated by magenta arrows, and (A) ChAT- or (B) TH-immunoreactive neurons are indicated by gray arrows. (Ai) Yellow-bordered image corresponds to the region within the yellow-dotted box. (Bii) Yellow-bordered image corresponds to the region within the yellow-dotted box. Scale bars = 20 μm . (C) Photomicrographs at (i–iii) low and (iv–vii) high magnification showing appositions (highlighted by green arrow heads) between colorectal-labeled fibers (CTB, magenta) and TH-immunoreactive neurons (gray) in the nucleus of the solitary tract (NTS). Scale bars: i–iii = 20 μm ; iv–vii = 10 μm . Photomicrographs are maximum z-projections from three to four confocal optical sections (0.5- to 2- μm -thick z-steps).

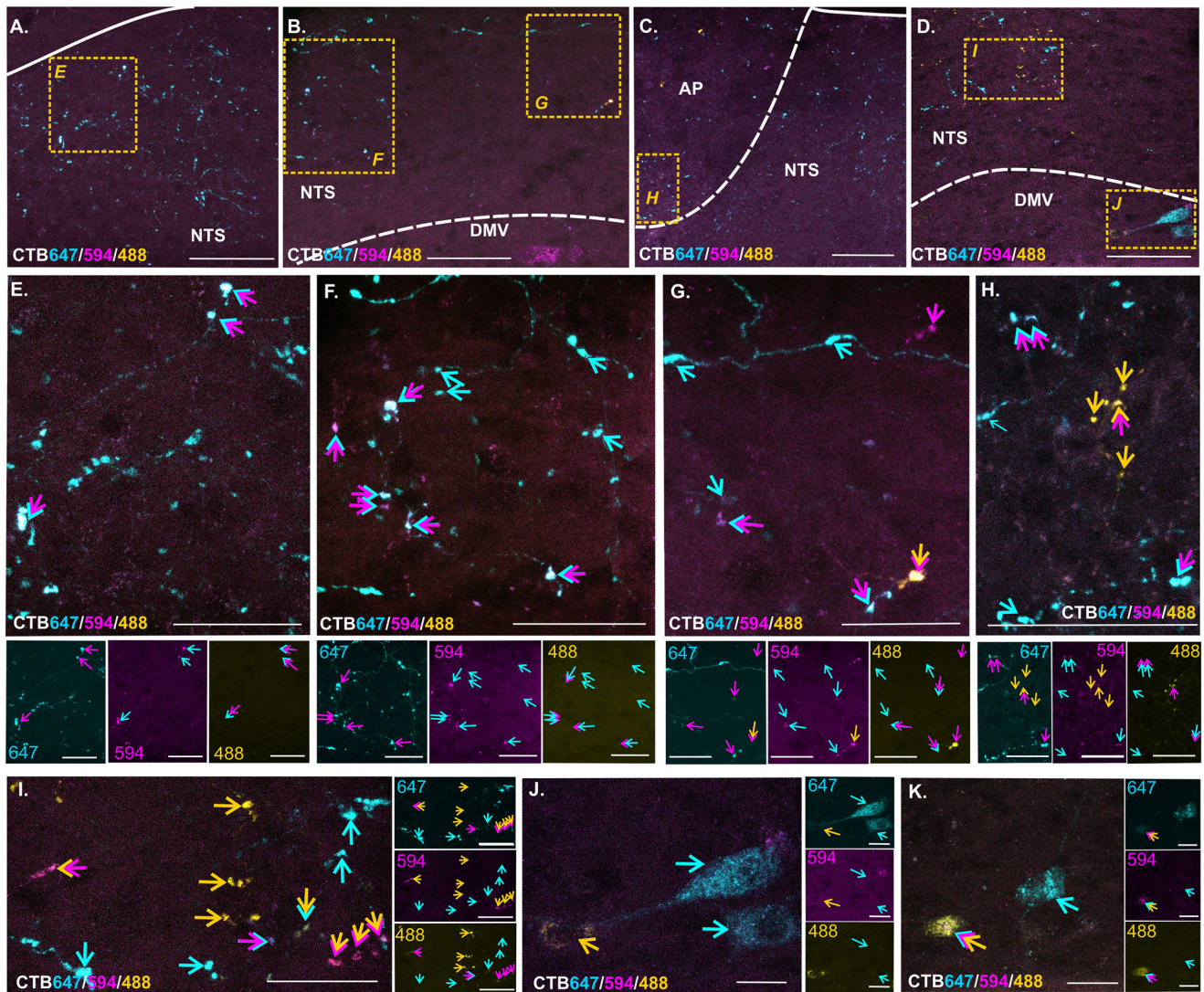


FIGURE 6 Distribution of retrograde-labeled fibers and cell bodies within the dorsal vagal complex (DVC) following colorectal regional tracing. Photomicrographs at (A–D) low and (E–K) high magnification showing the distribution of colorectal-labeled fibers in the (A–I) nucleus of the solitary tract (NTS) and (C and H) area postrema (AP) and (B, D, J, and K) cell bodies in the dorsal motor nucleus of the vagus (DMV) following injections of CTB-647 (cyan) into the rostral, CTB-594 (magenta) into the intermediate, and CTB-488 (yellow) into the caudal aspects of the colorectum. Labeled fibers and cell bodies are indicated by colored arrows: cyan = rostral CTB-647, magenta = intermediate CTB-594, and yellow = caudal CTB-488. Multiple headed arrows highlight fibers and cell bodies co-labeled from multiple injection sites. Scale bars: A–D = 50 μm ; E–K = 20 μm . Photomicrographs are maximum-intensity projections from confocal-collected six to nine optical sections (1- to 5- μm -thick z-intervals).

2.5 | Immunohistochemical identification of neurons activated by CRD and co-labeling for neurochemical markers

Primary and secondary antibodies used are outlined in Table 1. Immunofluorescence for pERK and neurochemical markers was performed as previously described (Grundy et al., 2018, 2019; Harrington et al., 2012, 2013, 2019). Immunolabeling for pERK using HRP-DAB detection (EnVision FLEX Mini Kit; Agilent) and the DAKO Omnis auto-stainer (Agilent Technologies Australia), followed by hematoxylin

staining, was performed as previously described (Castro et al., 2021; Grundy et al., 2020, 2021).

2.5.1 | pERK antibody

Rabbit monoclonal antibody detects endogenous levels of p44 and p42 MAP Kinase (Erk1 and Erk2) when dually phosphorylated at Thr202 and Tyr204 of Erk1 (Thr185 and Tyr187 of Erk2) and singly phosphorylated at Thr202. The antibody does not cross-react with

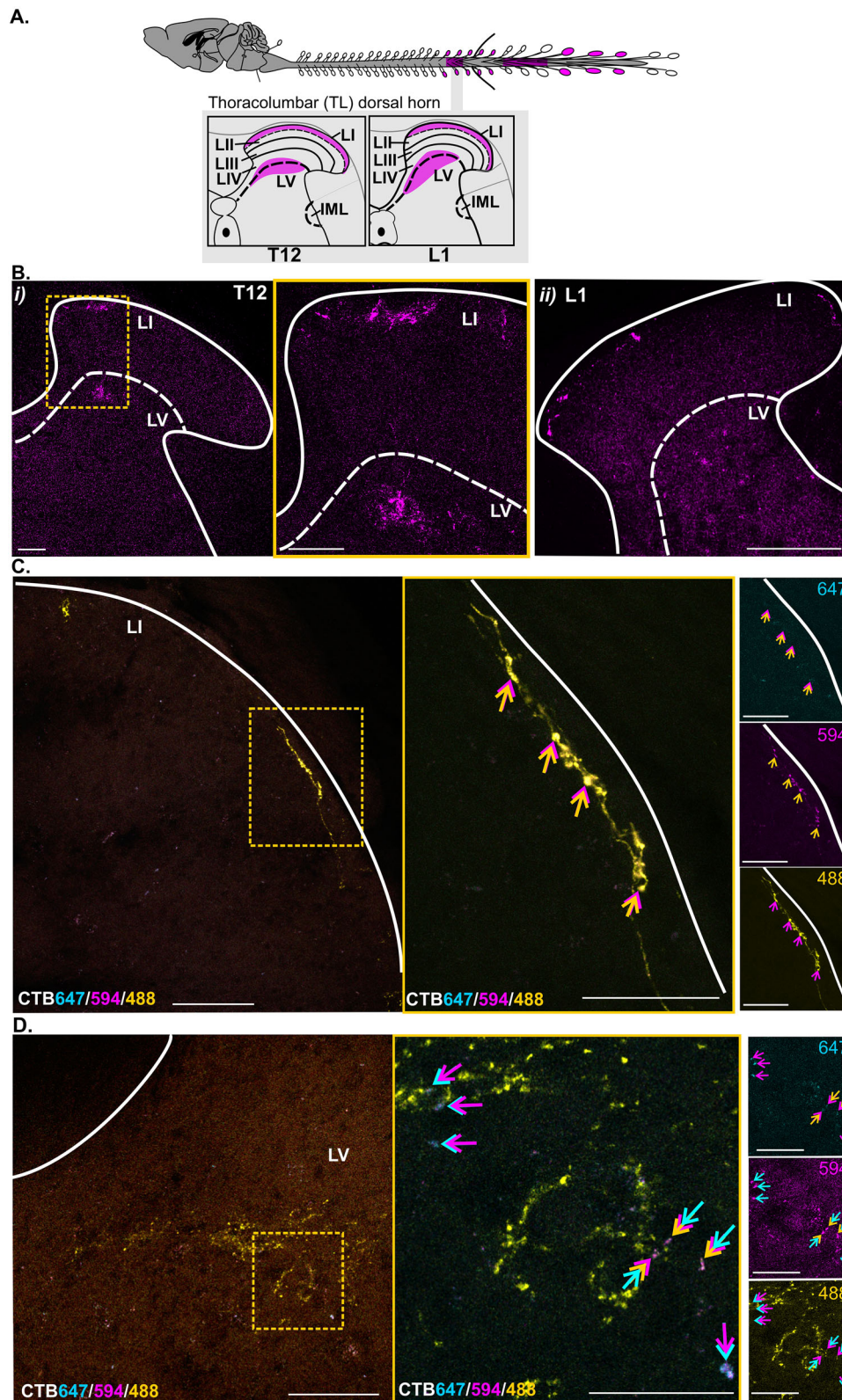


FIGURE 7 Distribution of colorectal retrograde-labeled fibers and cell bodies within the dorsal horn of the thoracolumbar (TL) spinal cord. (A) Schematic (Lein et al., 2007) illustrating the level of the thoracolumbar spinal cord (thoracic 12 [T12] and lumbar 1 [L1]) and regions of the dorsal horn in which labeled fibers (indicated by magenta shaded areas) were observed following colorectal retrograde tracing. Observations are from $N = 8$ mice (4 female, 4 male). (B) Photomicrographs of dorsal horn sections from (i) T12 and (ii) L1 spinal cord levels showing colorectal-labeled fibers (magenta) in lamina I (LI) and lamina V (LV). (i) Image in yellow-lined box corresponds to the region in the yellow-dotted box. Scale bars = 50 μm . (C, D) Photomicrographs showing the distribution of colorectal-labeled fibers in (C) LI and (D) LV following injections of CTB-647

(Continues)

FIGURE 7 (Continued)

(cyan) into the rostral, CTB-594 (magenta) into the intermediate, and CTB-488 (yellow) into the caudal aspects of the colorectum. Images in yellow-lined boxes (scale bars = 20 μm) correspond to the regions within the yellow-dotted boxes (scale bars = 50 μm). Labeled fibers are indicated by colored arrows: cyan = rostral CTB-647, magenta = intermediate CTB-594, and yellow = caudal CTB-488. Multiple headed arrows highlight fibers co-labeled from multiple injection sites. Photomicrographs are maximum-intensity projections from confocal-collected three to five optical sections (1- to 5- μm -thick z-intervals). Dashed lines indicate the dorsal border of lamina V (LV). LII, lamina 2; LIII, lamina 3; LIV, lamina 4; IML, intermediolateral column nuclei.

the corresponding phosphorylated residues of either JNK/SAPK or p38 MAP kinases (manufacturer's specifications) and binds specifically to a 44-kDa band in stimulated mouse tissue (Miyaji et al., 2009).

2.5.2 | Choline acetyltransferase, tyrosine hydroxylase, and calcitonin gene-related peptide antibodies

Optimal concentrations of antibodies were determined by serial dilutions. The goat anti-ChAT antiserum gave a pattern of labeling for cholinergic neurons in the mouse spinal cord and caudal medulla as previously reported (Gotts et al., 2016; Huffman et al., 2019; McGovern et al., 2010). The mouse monoclonal anti-TH antiserum used recognizes the 34-kDa catalytic core of tyrosine hydroxylase (TH) (manufacturer's specifications) and gave a pattern of labeling in the caudal medulla as previously described (Appleyard et al., 2007; Bassi et al., 2022). Specificity of the rabbit anti-CGRP serum has been confirmed in the rat amygdala and spinal cord using preabsorption control peptides (manufacturer's application notes and Harrington et al., 2012).

2.6 | Microscopy

Fluorescence was visualized using a confocal laser scanning microscope (Leica TCS SP8X). pERK-DAB staining was imaged using a NanoZoomer automated slide scanner (Hamamatsu) with a 40 \times objective. Confocal images (1024 \times 1024 pixels) were obtained with PL APO CS2 air 10 \times (for imaging of CLARITY-cleared ganglia) or oil immersion 20 \times , 40 \times , or 63 \times (spinal cord/medulla sections) objectives and software zoom of 2–4 \times magnification. Sequential scanning (five-line average) was performed with the following settings using a tunable white light laser and photomultiplier detectors: 495 nm excitation and 503/538 nm emission detection for AF488; 561 nm excitation and 570–625 nm emission detection for AF594; and 633 nm excitation with 642–750 nm emission settings for AF647. CLARITY-cleared ganglia were optically sectioned (10- μm thick) and z-projected images were reconstructed for each ganglion (230–390 μm). Spinal cord and medulla sections were optically sectioned (0.5- to 5- μm -thick sections) and maximum z-projected images were reconstructed (10–50 μm). Images were processed using LAS Lite (Leica), FIJI (NIH), and CorelDRAW Graphic Suite 2021 (Corel Corporation) software. Other than

making moderate adjustments for contrast and brightness, the images were not manipulated in any way.

2.7 | Neuronal counts and statistics

Neuronal counts were analyzed from saved digital photomicrographs. Only cells with a neuronal morphological profile and intact nuclei (identified by DAPI or hematoxylin counter stain) were included in the counts. All data were analyzed using GraphPad Prism 9. The data distribution was determined by the GraphPad Prism 9 normality and lognormality Shapiro–Wilk tests. The specific number of mice in each experimental group (*N*), the samples per mouse (*n*, ganglia, or sections), and details of the tests used for statistical comparisons between experimental groups are outlined within the relevant figure legends.

2.7.1 | Quantification of retrograde-labeled colonic afferent neurons CLARITY-cleared whole ganglia and sectioned ganglia

Labeled neurons were manually counted in CLARITY-cleared and sectioned ganglia, using Image J color channel and Cell Counter tools (Schneider et al., 2012).

2.7.2 | Quantification of pERK-immunoreactive neurons in ganglia, spinal cord, and medulla sections

Neuronal counts were performed on scanned images opened in digital pathology viewing software QuPath using the cell count function (Queens University) (Bankhead et al., 2017). Subregions of the dorsal horn and the DVC were based on the Allen Institute Mouse Spinal Cord Atlas (<https://mousespinal.brain-map.org/imageseries/showref.html>) and the Paxinos and Franklin Mouse Brain Atlas (Paxinos et al., 2001).

2.7.3 | Quantification of pERK-immunoreactive neurons in the dorsal horn LI and the DVC NTS labeled from the PbN

Neuronal counts were performed using Image J Cell Counter tools on confocally acquired single-plane images of TL and LS dorsal horn and medulla DVC.

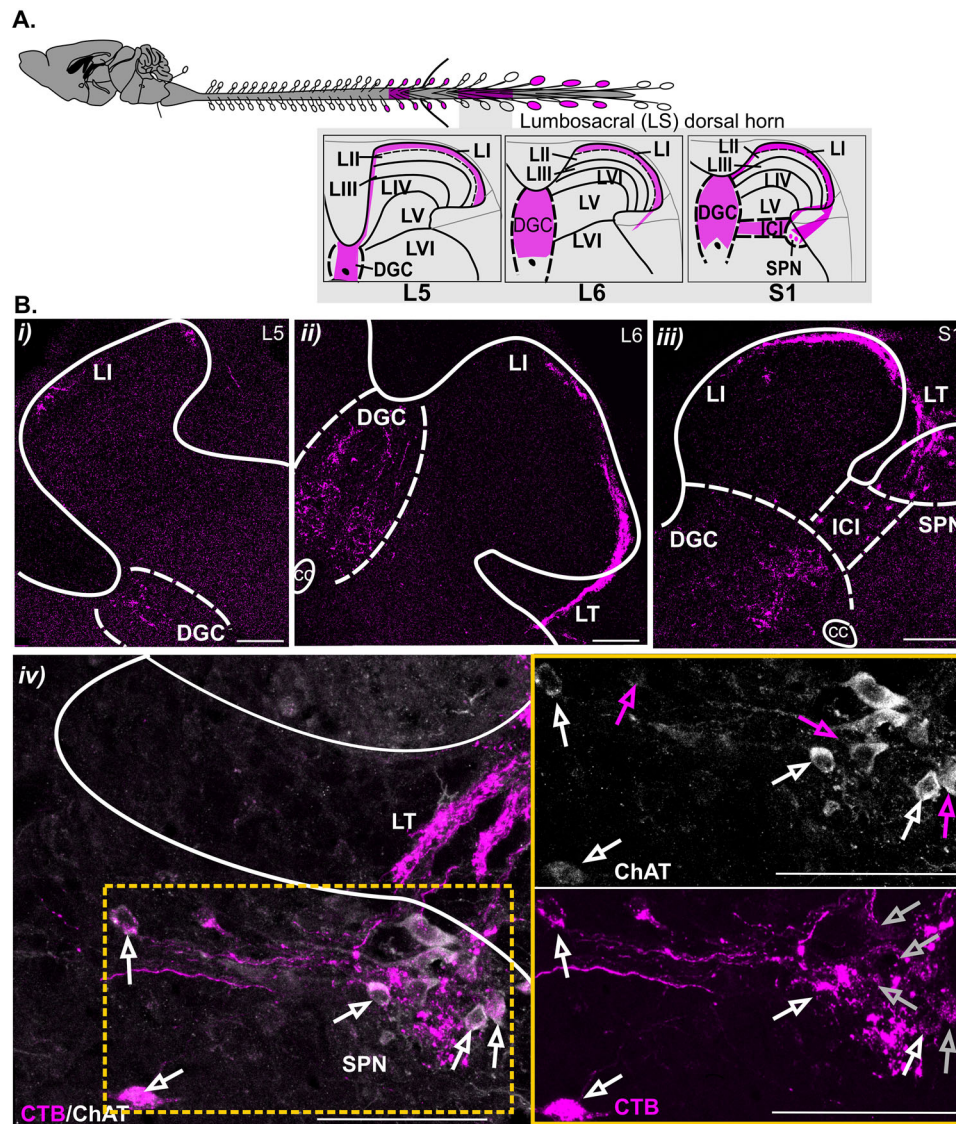


FIGURE 8 Distribution of colorectal retrograde-labeled fibers and cell bodies within the dorsal horn of the lumbosacral (LS) spinal cord. (A) Schematic (Lein et al., 2007) illustrating the level of the lumbosacral spinal cord (lumbar 5 [L5], lumbar 6 [L6], and sacral 1 [S1]) and regions of the dorsal horn in which labeled fibers and cell bodies (indicated by magenta shaded areas) were observed following colorectal retrograde tracing. Observations are from $N = 8$ mice (4 female, 4 male). (B) Photomicrographs of dorsal horn at (i) L5, (ii) L6, and (iii) and (iv) S1 spinal cord levels showing the distribution of colorectal-labeled fibers and cell bodies (magenta). (iv) Photomicrograph showing the distribution of colorectal-labeled fibers and cell bodies (CTB, magenta) relative to ChAT-immunoreactive (-IR) neurons (ChAT, gray) within the sacral parasympathetic nuclei (SPN). ChAT-IR neurons are indicated by gray arrows, colorectal-labeled neurons are indicated by magenta arrows, and co-labeled neurons are indicated by white arrows. Image in the yellow-lined box corresponds to the region outlined by the yellow-dotted box. Scale bars: i-iii = 100 μm ; iv = 50 μm . Photomicrographs are maximum-intensity projections from confocal-collected five optical sections (1- to 5- μm -thick z-intervals). Dashed lines indicate the lateral borders of the dorsal gray commissure (DGC), SPN, and the intercalated nucleus (ICI). cc, central canal; LT, lateral tracts; LII, lamina 2; LIII, lamina 3; LIV, lamina 4; LV, lamina 5; LVI, lamina 6.

3 | RESULTS

3.1 | The distribution and relative abundance of sensory neurons retrogradely labeled from the distal colon and rectum (colorectum) in vagal and spinal afferent pathways

The total number of neurons labeled from colorectal retrograde tracing, using multiple injections of CTB-594 (Figure 1Ai), was compared

between whole VG and DRG (at various spinal levels; Figure 1Aii). Colorectal-labeled neurons were observed within the VG (Figure 1Bi) and within DRG at thoracic (T12, T13; Figure 1Bii,iii), lumbar (L1, L5, and L6; Figure 1Biv,vi,vii), and sacral (S1; Figure 1Bviii) spinal levels. Labeled neurons were rare (Figure 1Ci), or absent, in DRG at T9 and L2 through to L4 (Figure 1Bv) spinal levels. L6 DRG contained the greatest number of labeled neurons relative to all other ganglia in which labeled neurons were observed (Figure 1Ci). Upon comparing the number of colorectal-labeled neurons between primary afferent pathways,

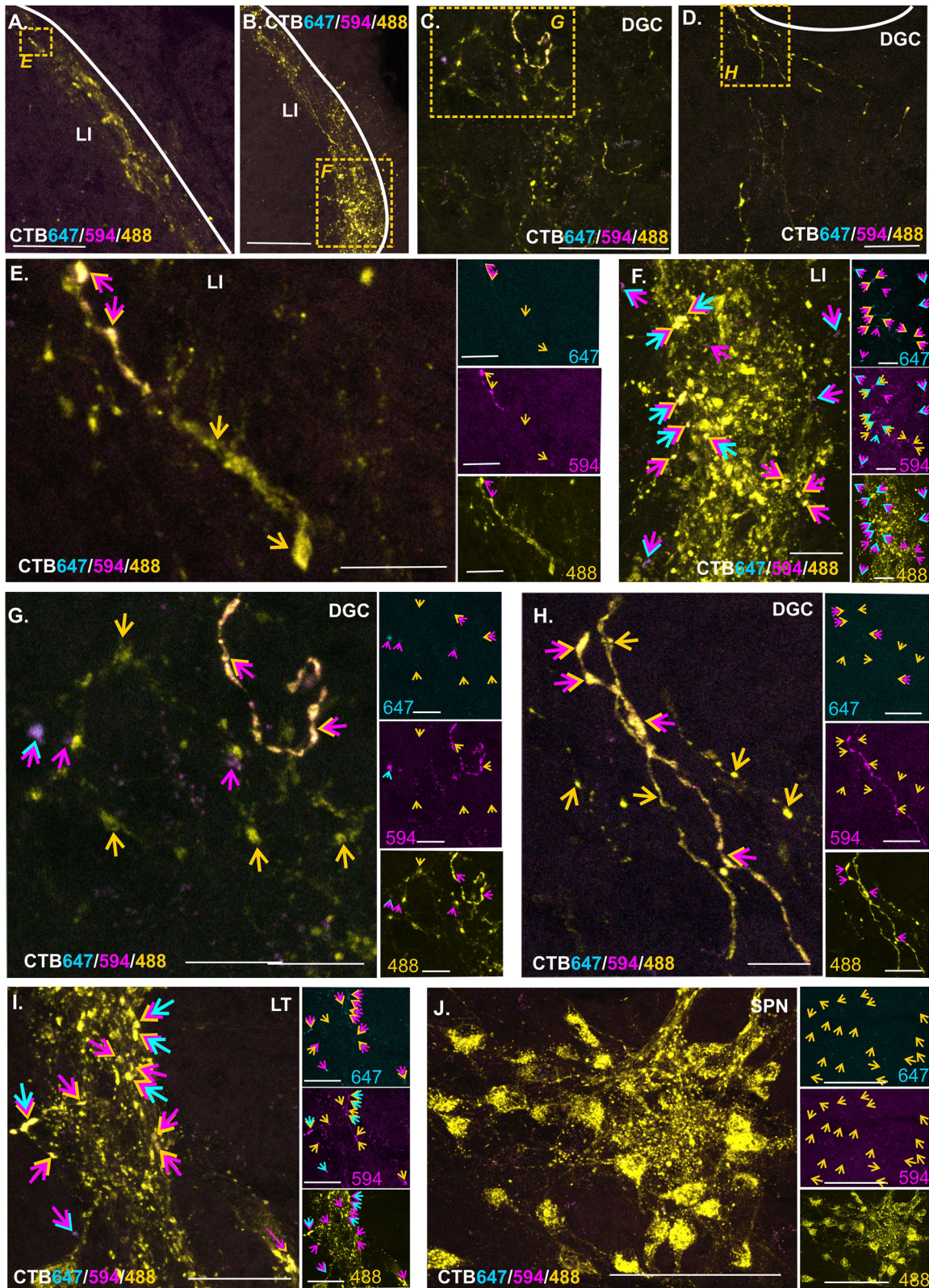


FIGURE 9 Distribution of retrograde-labeled fibers and cell bodies within the lumbosacral (LS) spinal cord dorsal horn following colorectal regional tracing. Photomicrographs at (A–D) low and (E–J) high magnification of (A, B, E, and F) lamina I (LI), (C, D, G, and H) the dorsal gray commissure (DGC), (I) lateral tracts (LT), and (J) the sacral parasympathetic nucleus (SPN) following injections of CTB-647 (cyan) into the rostral, CTB-594 (magenta) into the intermediate, and CTB-488 (yellow) into the caudal aspects of the colorectum. Labeled fibers and cell bodies are indicated by colored arrows: cyan = rostral CTB-647, magenta = intermediate CTB-594, and yellow = caudal CTB-488. Multiple headed arrows highlight fibers co-labeled from multiple injection sites. Scale bars = A–D and J = 50 μm ; E–I = 10 μm . Photomicrographs are maximum-intensity projections from confocal-collected six to 10 optical sections (0.5- to 5- μm -thick z-intervals).

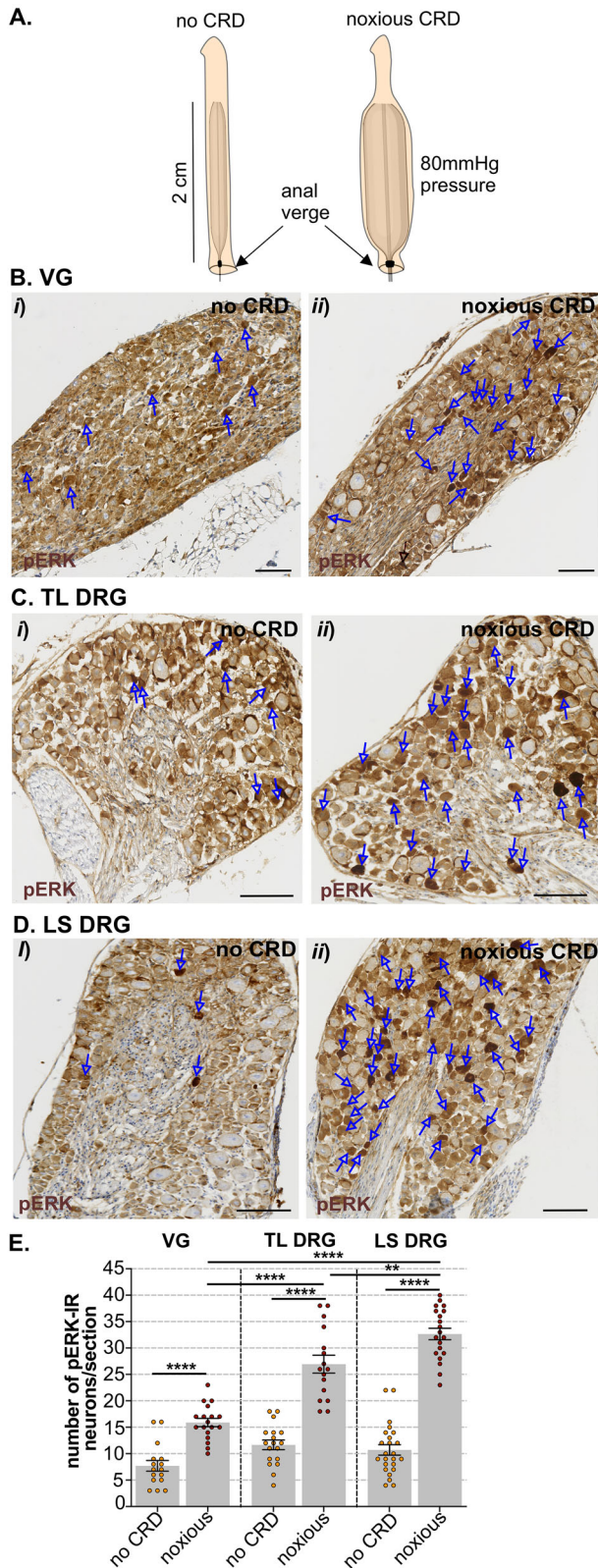


FIGURE 10 Comparison of the number of pERK-immunoreactive (pERK-IR) neurons following noxious colorectal distension between nodose/jugular ganglia (VG) and spinal dorsal root ganglia (DRG). (A) Schematic illustration of the placement of a 2-cm-long balloon catheter within the colorectum (0.2 cm from the anal verge) that was

(Continues)

FIGURE 10 (Continued)

not inflated (no CRD) or inflated to a pressure of 80 mmHg (noxious CRD). (B–D) Photomicrographs showing pERK-IR neurons (pERK, brown, indicated by blue arrows) in the (B) VG, (C) TL (T10–L1) DRG, and (D) LS (L5–S1) DRG sections from mice that underwent (i) no CRD or (ii) noxious CRD. Scale bars = 100 μ m. (E) Quantification of the number of pERK-IR neurons following no CRD or noxious CRD within individual sections of VG, TL DRG, and LS DRG. $**p < .01$ and $****p < .0001$, determined by one-way ANOVA (parametric data) with Bonferroni multiple comparison tests. Individual data points represent the number of pERK-IR neurons/section, with 3–6 sections/mouse from $N = 4$ male mice.

vagal (VG), splanchnic (TL DRG; T10–L1), and pelvic (LS DRG; L5–S1), the pelvic pathway contained the most labeled neurons, followed by splanchnic and then vagal (Figure 1Ci). There was no significant difference between male and female mice in the number of colorectal CTB-594-labeled neurons at the individual ganglia level (Figure 1Di) or at the afferent pathway level (Figure 1Dii).

Retrograde tracing using different CTB-AF injected into three regions of the colorectum (Figure 2A) identified a rostral-caudal (i.e., proximal–distal) gradient of vagal and spinal (splanchnic and pelvic) afferent innervation of the colorectum (Figure 2B–E). The abundance of CTB-647-, CTB-594-, or CTB-488-labeled neurons varied between the VG (Figure 2Bi–iv), TL DRG (Figure 2Ci–iv), and LS DRG (Figure 2Di–iv), reflecting the rostral–caudal location of CTB injection. Neurons in the VG were predominantly labeled from rostrally injected CTB-647 (Figure 2Bi,v), while only a minor proportion were labeled from caudally injected CTB-488 (Figure 2Biii,v). In the TL DRG, neurons labeled from rostrally (Figure 2Ci), intermediately (Figure 2Cii), or caudally (Figure 2Ciii) injected CTB were in relatively even proportions (Figure 2Cv). In the LS DRG, very few neurons were labeled from rostrally injected CTB-647 only (Figure 2Di,v) relative to those labeled from only caudally injected CTB-488 (Figure 2Diii,v). Neurons co-labeled from two or more injection sites were observed in each ganglion (Figure 2Biv,Civ,Div) and accounted for approximately 39% of labeled neurons within the VG (Figure 2Bv) and 45% within the TL DRG (Figure 2Cv), but only 15% within the LS DRG (Figure 2Dv). Quantification of the number of neurons labeled by either CTB-647 (Figure 2Ei), CTB-594 (Figure 2Eii), or CTB-488 (Figure 2Eiii) or co-labeled (Figure 2Eiv) highlighted that rostrally injected CTB-647 labeled significantly more neurons in the VG, relative to TL and LS DRG (Figure 2Ei). Similar numbers of neurons across VG, TL, and LS DRG were labeled from intermediately injected CTB-594 (Figure 2Eii), while caudally injected CTB-488 labeled significantly more neurons in the LS DRG, relative to the VG and TL DRG (Figure 2Eiii). Neurons co-labeled from rostral CTB-647 and intermediate CTB-594 injections were most common in the VG (Figure 2Eiv), whereas neurons labeled from intermediate CTB-594 and caudal CTB-488 injections were most common in the LS (Figure 2Eiv). Neurons co-labeled from all three injection sites were observed in each ganglion, although neurons co-labeled from rostral CTB-647 and caudal CTB-488 injections were rarely observed (Figure 2Eiv).

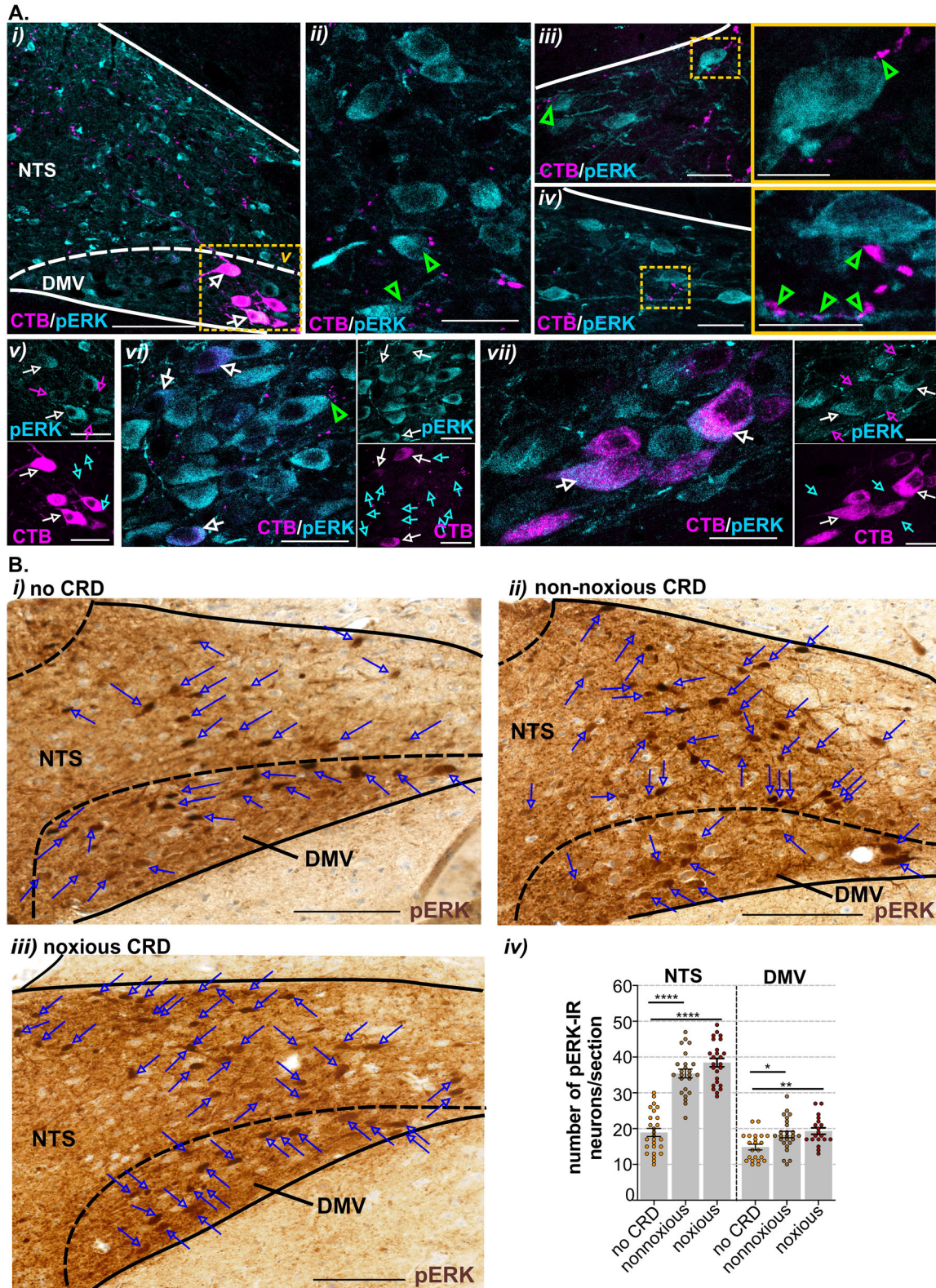


FIGURE 11 Spatial correlation between the distribution of colorectal-labeled fibers and pERK-immunoreactive (pERK-IR) neurons in the dorsal vagal complex (DVC) following colorectal distension (CRD). (A) Photomicrographs of the (i–iv) nucleus of the solitary tract (NTS) and (i, v, and vii) dorsal motor nucleus of the vagus (DMV) showing the distribution of colorectal retrograde-labeled (i–iv and vi) fibers and (i, v, and vii) cell bodies (magenta) in relation to pERK-IR neurons (pERK, cyan) following noxious CRD. (i–iv and vi) pERK-IR neurons in apposition to colorectal-labeled fibers are highlighted by green arrow heads. (iii and iv) High-magnification images (scale bars = 10 μ m) bordered by yellow lines correspond to regions within yellow-dotted boxes. (v–vii) Colorectal-labeled cell bodies in the DMV are indicated by magenta arrows, pERK-IR

(Continues)

FIGURE 11 (Continued)

neurons are indicated by cyan arrows, and co-labeled neurons are indicated by white arrows. Images in (v) correspond to the region within the yellow dotted box in (i). Scale bars: i = 100 μm ; ii–vii = 20 μm . Photomicrographs are reconstructions from confocal-collected three to four optical sections (2- μm -thick z-steps). (B) Photomicrographs of DVC showing the distribution of pERK-IR neurons (brown, indicated by blue arrows) in the NTS and DMV following (i) no CRD, (ii) nonnoxious CRD, and (iii) noxious CRD. Scale bars = 100 μm . (iv) Quantitative data gained from caudal medulla DVC sections (spanning -7.5 to -7.7 caudal to bregma) comparing the number of pERK-IR neurons in the NTS and the DMV following no CRD, nonnoxious CRD, and noxious CRD. * $p < .05$, ** $p < .01$, and **** $p < .0001$, determined by one-way ANOVA (parametric data) with Tukey's multiple comparison tests. Individual data points represent the number of pERK-IR in a section, and error bars represent the standard error of the mean, gained from 3–4 (caudal medulla) sections/mouse from $N = 9$ mice (4 male, 5 female) no CRD, $N = 8$ mice (4 male, 4 female) nonnoxious CRD, and $N = 9$ mice (5 male, 4 female) noxious CRD.

3.2 | Organization of colorectal retrograde-labeled afferent central projections and parasympathetic motor neurons in the caudal medulla DVC

Within the caudal medulla DVC (Figure 3A), colorectal-labeled fibers were observed within the NTS (Figure 3Bi–vi) and in the AP (Figure 3Bi,ii,iv). Labeled fibers, although sparse, were also observed within the dorsal motor nucleus of the vagus (DMV), in addition to labeled cell bodies (Figure 3Bi–iii,vi). In the NTS, colorectal-labeled fibers were evident within the commissural and dorsolateral aspects of the NTS, where calcitonin gene-related peptide (CGRP)-immunoreactive fibers were prominent (Figure 4A). However, colorectal-labeled fibers were not CGRP immunoreactive (Figure 4Bi–iii). Colorectal-labeled cell bodies in the DMV were immunoreactive for choline acetyltransferase (ChAT) (Figure 5Ai–ii), but not TH (Figure 5Bi,ii). Within the NTS, retrograde-labeled fibers were observed in apposition to populations of TH-immunoreactive cell bodies and their processes (Figure 5Ci–vii). Following regional colorectal tracing, labeled fibers from rostrally injected CTB-647 were prominent within the NTS and AP (Figure 6A–I). Fibers labeled from the intermediately injected CTB-594 or caudally injected CTB-488 were sparse relative to CTB-647-labeled fibers; however, they were still evident within the AP (Figure 6C,H) and the NTS (Figure 6D,I). Co-labeled fibers from either rostral 647/intermediate 594 injections or intermediate 594/caudal 488 injections were also evident in the NTS (Figure 6E–I). Cell bodies labeled from caudally injected CTB-488, rostral CTB-647 or intermediate CTB-594, or co-labeled by all three injection sites were evident in the DMV (Figure 6B,D,J,K).

3.3 | Organization of colorectal retrograde-labeled afferent central projections and parasympathetic motor neurons in the spinal cord dorsal horn

Aligning with the distribution of colorectal-labeled neurons within DRG at certain spinal levels, colorectal-labeled fibers were localized within the dorsal horn at specific levels of the TL (Figure 7) and LS (Figures 8 and 9) spinal cord. In the TL spinal cord (Figure 7A), colorectal-labeled fibers projected within dorsal horn LI and LV (Figure 7Bi,ii). Following regional retrograde tracing, fibers

labeled from caudally injected CTB-488 only were evident within LI (Figure 7C) and LV (Figure 7D), as well as fibers co-labeled from either rostral 647/intermediate 594 injections (Figure 7D), intermediate 594/caudal 488 (Figure 7C), or all three injection sites (Figure 7D).

In the LS spinal cord (Figure 8A), labeled fibers were observed at L5 (Figure 8Bi), L6 (Figure 8Bii), and S1 (Figure 8Biii,iv) spinal levels—specifically, within the dorsal horn LI–II (Figure 8Bi–iii), within the dorsal gray commissure (DGC) (Figure 8Bi–iii), and projecting within lateral collateral tracts (Figure 8Bii–iv). In the sacral spinal cord, fibers in the lateral tracts projected into the SPN, which was identified by the presence of ChAT-immunoreactive cell bodies of parasympathetic pre-ganglionic motor neurons (Figure 8Biv). In addition to fibers, colorectal-labeled cell bodies were also evident within the SPN (Figure 8Biii,iv), populations of which were ChAT immunoreactive (Figure 8Biv). Following regional retrograde tracing, in the LS dorsal horn (Figure 9), labeling from caudally injected CTB-488 was abundant within LI (Figure 9A,B,E,F), the DGC (Figure 9C,D,G,H), lateral tracts (Figure 9I), and the SPN (Figure 9J). Fibers co-labeled from rostral CTB-647/intermediate CTB-594, intermediate CTB-594/caudal-488, or all three injection sites were sparse in LI (Figure 9E,F), the DGC (Figure 9G,H), and lateral tracts (Figure 9I). Fiber labeling from only intermediately injected CTB-594 or rostrally injected CTB-647 was rare. Cell bodies in the SPN were only labeled from caudally injected CTB-488 (Figure 9J).

3.4 | Comparison of CRD evoked neuronal activation between vagal and spinal afferent pathways

The number of pERK-immunoreactive (pERK-IR) neurons following in vivo noxious CRD (Figure 10A) was compared among the VG (Figure 10B), TL (Figure 10C), and LS (Figure 10D) DRG. Relative to no CRD controls, noxious CRD significantly increase the number of pERK-IR neurons in each ganglion (Figure 10E). Aligning with observations from colorectal retrograde tracing, the number of pERK-IR neurons following noxious CRD observed within the LS DRG was significantly greater than that in the TL and VG. Furthermore, the number of pERK-IR neurons in the TL DRG was significantly greater than that observed in the VG (Figure 10E).

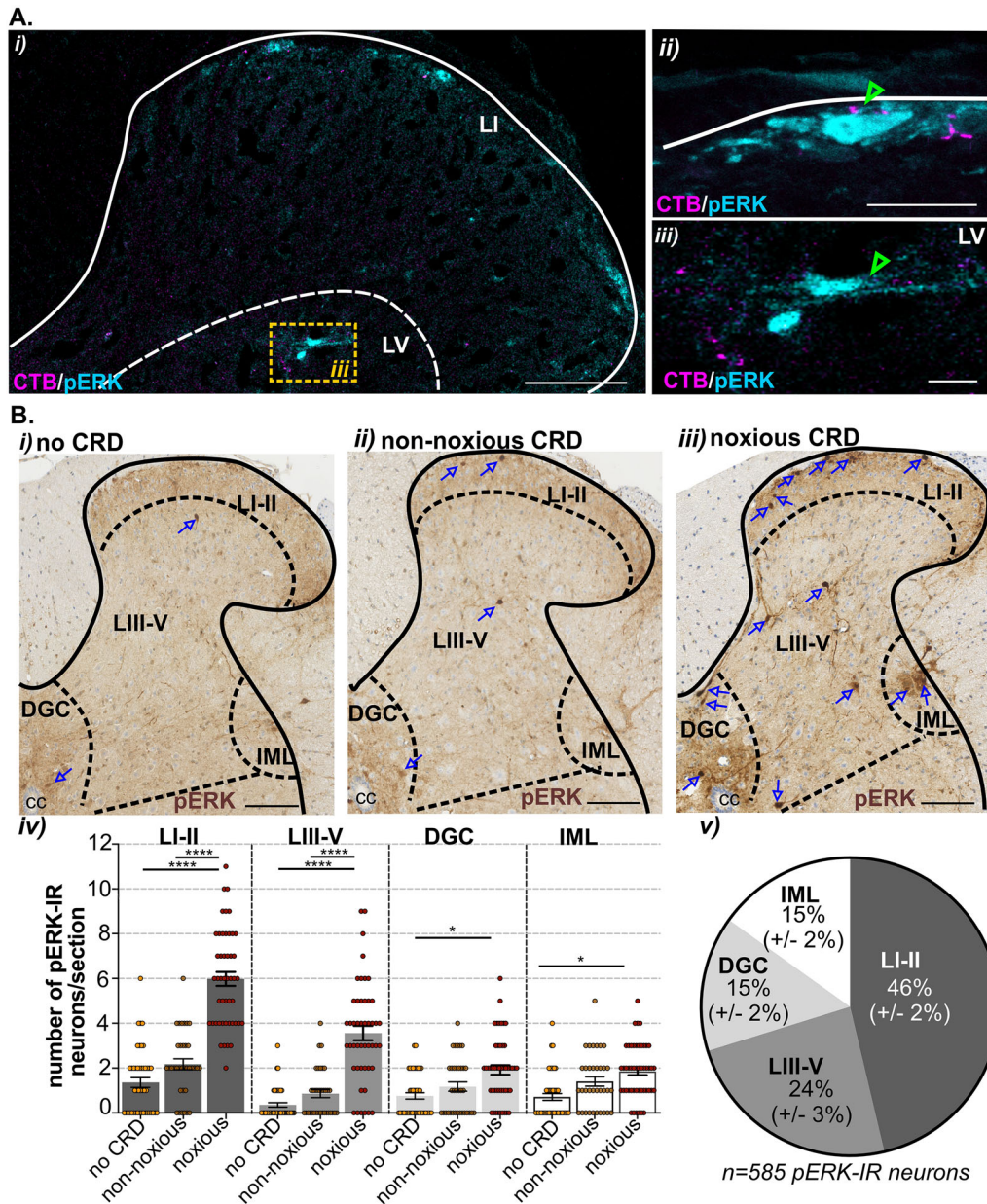


FIGURE 12 Spatial correlation between the distribution of colorectal-labeled fibers and pERK-immunoreactive (pERK-IR) neurons in the thoracolumbar spinal cord dorsal horn following colorectal distension (CRD). (A) Photomicrographs showing the distribution of colorectal retrograde-labeled fibers (magenta) in relation to neurons immunoreactive for pERK (cyan) in the dorsal horn (i and ii) lamina I (LI) and (i and iii) lamina V (LV) in the thoracic T13 spinal cord following noxious CRD. pERK-IR neurons in apposition to colorectal-labeled fibers are highlighted by green arrow heads. Images in (iii) correspond to the region within the yellow-dotted box in (i) at higher magnification. Scale bars: i = 500 μm ; ii and iii = 20 μm . Photomicrographs are reconstructions from confocal-collected three to four optical sections (2- μm -thick z-steps). (B) Photomicrographs of dorsal horn at thoracic T13 spinal level showing the distribution of pERK-IR neurons (brown, indicated by blue arrows) in superficial laminae I–II (LI–II), deep laminae (LIII–V), the dorsal gray commissure (DGC), and the intermediolateral column nuclei (IML) following (i) no CRD, (ii) nonnoxious CRD, and (iii) noxious CRD. Scale bars = 100 μm . (iv) Quantitative data obtained from dorsal horn sections covering T13–L1 spinal levels comparing the number of pERK-IR neurons per section in dorsal horn subregions LI–II (dark gray bars), LIII–V (mid-gray bars), DGC (light gray bars), and the IML (white bars) following no CRD, nonnoxious CRD, and noxious CRD. * $p < .05$ and **** $p < .0001$, determined by a Kruskal–Wallis ANOVA test (nonparametric) with Dunn’s multiple comparison tests. (v) Quantitative data showing the mean (\pm standard error of the mean) proportion of pERK-IR neurons per section in each of the dorsal horn subregions (LI–LII, LIII–IV, DGC, and IML) following noxious CRD. Individual data points represent the number of pERK-IR in a section, and error bars represent the standard error of the mean, gained from 5–6 sections/mouse from $N = 10$ mice (5 male, 5 female) no CRD, $N = 8$ mice (4 male, 4 female) nonnoxious CRD, and $N = 10$ mice (5 male, 5 female) noxious CRD. Dashed lines indicate borders of dorsal horn subregions used for quantification comparisons. DGC, dorsal gray commissure; LI, lamina 1; LII, lamina 2; LIII, lamina 3; LIV, lamina 4; LV, lamina 5; IML, intermediolateral column nuclei.

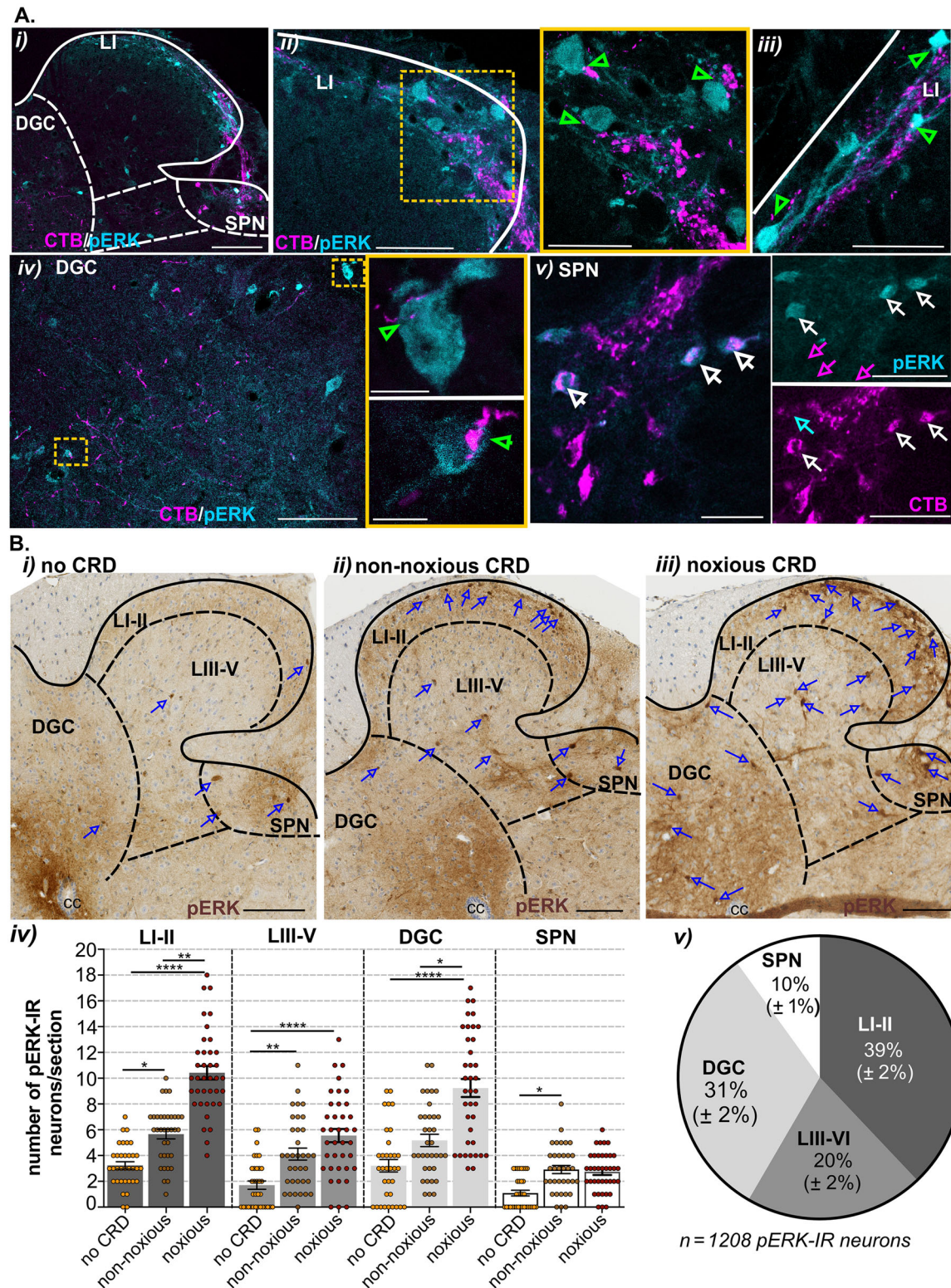


FIGURE 13 Spatial correlation between the distribution of colorectal-labeled fibers and pERK-immunoreactive (pERK-IR) neurons in the lumbosacral spinal cord following colorectal distension (CRD). (A) Photomicrographs showing the distribution of colorectal retrograde-labeled fibers (magenta) in relation to the distribution of neurons immunoreactive for pERK (cyan) in the sacral spinal cord (i) dorsal horn, (i–iii) lamina I (LI), (i and iv) the dorsal gray commissure (DGC), and the (i and v) sacral parasympathetic nuclei (SPN) following noxious CRD. (ii–iv) Green arrow heads highlight pERK-IR neurons in apposition to colorectal-labeled fibers. (iii) Image in yellow-lined box (scale bar = 20 μ m) corresponds to the region within the yellow-dotted box (scale bar = 50 μ m). (iv) Images in yellow-lined boxes (scale bar = 10 μ m) correspond to the regions in

(Continues)

FIGURE 13 (Continued)

yellow-dotted boxes within the DGC (scale bar = 50 μm). (v) Colorectal-labeled cell bodies in the SPN are indicated by magenta arrows, pERK-IR neurons are indicated by cyan arrows, and co-labeled neurons are indicated by white arrows. Scale bars: i = 100 μm ; iii and v = 20 μm . (B) Photomicrographs of dorsal horn at sacral S1 spinal level showing the distribution of pERK-IR neurons (brown, indicated by blue arrows) in superficial laminae I–II (LI–LII), deep laminae (LIII–V), the dorsal gray commissure (DGC), and the sacral parasympathetic nucleus (SPN) following (i) no CRD, (ii) nonnoxious CRD, and (iii) noxious CRD. Scale bars = 100 μm . (iv) Quantitative data gained from S1 dorsal horn sections comparing the number of pERK-IR neurons per section in dorsal horn subregions LI–II (dark gray bars), LIII–V (mid-gray bars), DGC (light gray bars), and the SPN (white bars) following no CRD, nonnoxious CRD, and noxious CRD. * $p < .05$, ** $p < .01$, and **** $p < .0001$, determined by a Kruskal–Wallis test (all data nonparametric) with Dunn’s multiple comparison tests. (v) Quantitative data showing the mean (\pm standard error of the mean) proportion of pERK-IR neurons per section in each of the dorsal horn subregions following noxious CRD. Individual data points represent the number of pERK-IR in a section, and error bars represent the standard error of the mean, gained from 5–6 sections/mouse from $N = 10$ mice (5 male, 5 female) no CRD, $N = 8$ mice (4 male, 4 female) nonnoxious CRD, and $N = 10$ mice noxious CRD (5 male, 5 female). Dashed lines indicate borders of dorsal horn subregions used for quantification comparisons. cc, central canal; LII, lamina 2; LIII, lamina 3; LIV, lamina 4; LV, lamina 5.

The spatial correlation of colorectal-labeled fibers to CRD activated neurons was then assessed in the DVC (Figure 11), and TL (Figure 12), and LS (Figure 13) dorsal horn. In the DVC (Figure 11), pERK-IR neurons were distributed within the NTS (Figure 11Ai–iv) and the DMV (Figure 11Ai,Av–vii). Colorectal-labeled fibers in apposition to pERK-IR cell bodies and processes were observed in the NTS (Figure 11Aii–iv) and the DMV (Figure 11Avi). In the DMV, retrograde-labeled cell bodies were not all pERK-IR (Figure 11Ai,v–vii). Relative to no CRD (Figure 11Bi), nonnoxious CRD (Figure 11Bii) evoked a significant increase in the number of pERK-IR neurons in the NTS and the DMV (Figure 11Biv). In contrast, noxious CRD (Figure 11Biii) did not evoke an increase in the number of pERK-IR neurons in the NTS or DMV over that of nonnoxious CRD (Figure 11Biv).

In the TL dorsal horn (Figure 12), following noxious CRD, the distribution of pERK-IR neurons within the dorsal horn LI (Figure 12Ai,ii) and LV (Figure 12Ai,iii) correlated with the distribution of colorectal-labeled fibers. Relative to no CRD (Figure 12Bi) and nonnoxious CRD (Figure 12Bii), noxious CRD (Figure 12Biii) evoked a significant increase in the number of pERK-IR neurons within LI–II and LIII–V (Figure 12Biv). As a proportion of the total number of pERK-IR neurons in the TL dorsal horn following noxious CRD, the majority were localized within LI–II (Figure 12Bv).

In the LS dorsal horn (Figure 13), following noxious CRD, pERK-IR neurons were distributed throughout the dorsal horn LI–LV, the DGC, and the SPN (Figure 13Ai). pERK-IR neurons in apposition to colorectal fibers were evident in LI (Figure 13Ai–iii) and the DGC (Figure 13Ai,iv). Similar to the DMV, not all retrograde-labeled cell bodies in the SPN (Figure 13Ai,v) were pERK-IR following noxious CRD. Unlike the TL spinal cord, relative to no CRD (Figure 13Bi), nonnoxious CRD (Figure 13Bii) evoked a significant increase in the number of pERK-IR neurons (Figure 13Biv) in LI–II, LIII–V, and the SPN. Upon noxious CRD (Figure 13Biii), the number of pERK-IR neurons increased in LI–II and the DGC over that observed following nonnoxious CRD (Figure 13Biv). Following noxious CRD, pERK-IR neurons were evenly distributed within the LI–II and the DGC (Figure 13Biii,v). Upon comparing between male and female mice, no significant difference was

observed in the distribution (Figure 14Ai,ii) of pERK-IR neurons in the dorsal horn, nor the number of pERK-IR neurons following nonnoxious (Figure 14Bii,Cii) and noxious (Figure 14Biii,Ciii) CRD. However, in no CRD controls, female mice had greater numbers of pERK-IR neurons in LIII–V of the TL (Figure 14Bi) and LS dorsal horn (Figure 14Ci) compared to male mice. The number of pERK-IR neurons evoked by nonnoxious or noxious CRD in the NTS (Figure 14Di) or the DMV (Figure 14Dii) did not significantly differ between female and male mice.

3.5 | Comparison of CRD-evoked neuronal activation relayed into the PbN from vagal and spinal afferent pathways

Retrograde tracing from the PbN (Figure 15A) was combined with either colorectal retrograde tracing or in vivo noxious CRD to compare the spatial relationship between colorectal afferent projections and PbN-projecting neurons, and the number of CRD-activated neurons projecting to the PbN, between the vagal and the different spinal pathways. In the NTS (Figure 15B), colorectal-labeled fibers were in apposition to populations of PbN-labeled neurons (Figure 15Bi–iv), while PbN-projecting neurons accounted for a small proportion of pERK-IR neurons (Figure 15Ci–iv). In the TL dorsal horn (Figure 16), colorectal-labeled fibers were observed in apposition to PbN-retrograde-labeled neurons in LI (Figure 16Ai–iii). Correspondingly, pERK-IR PbN-labeled neurons were localized to LI (Figure 16Bi–iv), with PbN-labeled neurons accounting for a large proportion of the total pERK-IR neurons (Figure 16Bv). In contrast, in the LS dorsal horn (Figure 17), while colorectal-labeled fibers were observed in proximity to PbN-labeled neurons in LI (Figure 17Ai,ii), the majority of pERK-IR neurons in LI were not co-labeled from the PbN (Figure 17Bi–iv). In the LS dorsal horn, PbN-labeled neurons and colorectal-labeled fibers were also observed in proximity to each other within the DGC (Figures 17Ai and 18A) and the SPN (Figure 18C). However, unlike in the LI, PbN-labeled neurons in the DGC (Figure 18Bi,ii) or the SPN (Figure 18Di,ii) were pERK-IR following noxious CRD.

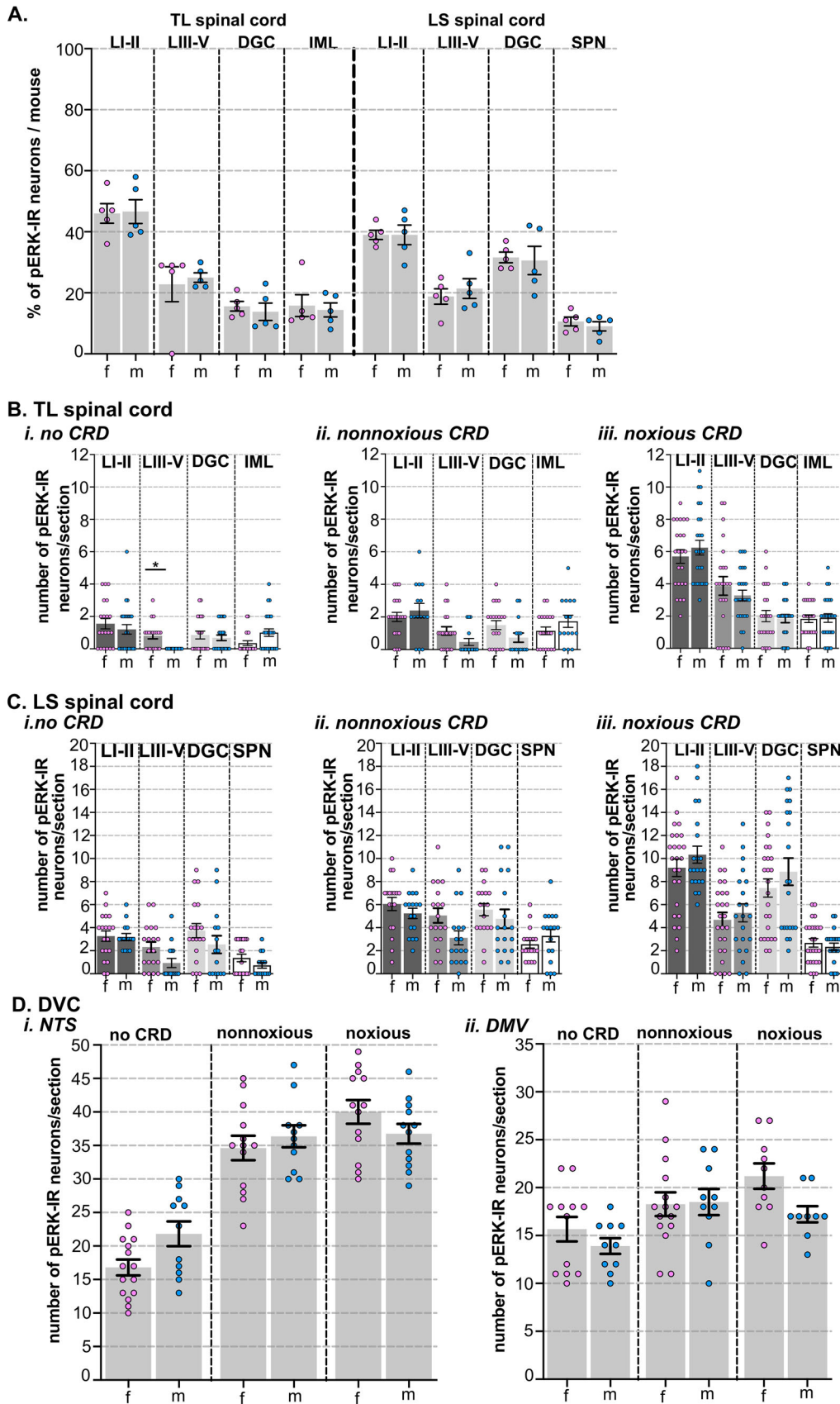


FIGURE 14 Female and male comparison of pERK-IR neurons in the spinal cord dorsal horn and caudal medulla DVC evoked by colorectal distension (CRD). (A) Quantitative data gained from dorsal horn sections covering TL spinal cord (T13–L1 spinal levels) and LS spinal cord (S1

(Continues)

FIGURE 14 (Continued)

spinal level) comparing the mean proportion of pERK-IR neurons per section in each of the dorsal horn subregions following noxious CRD per mouse between female (f; pink dots, $N = 5$) and male (m; blue dots, $N = 5$) mice. Collectively, the data show that there was no significant difference between female and male mice in the distribution of pERK-IR neurons following noxious CRD in either the TL or LS dorsal horn. Significance assessed by a one-way ANOVA (parametric data, standard deviations not significantly different) with Tukey's multiple comparison tests. Error bars represent the standard error of the mean. (B) Quantitative data gained from dorsal horn sections covering TL spinal cord (T13–L1 spinal levels) comparing the number of pERK-IR neurons per section in each of the dorsal horn subregions (LI–II [dark gray bars], LIII–V [mid-gray bars], DGC [light gray bars], and the IML [white bars]) following (i) no CRD, (ii) nonnoxious CRD, and (iii) noxious CRD between female (f; pink dots) and male (m; blue dots) mice. Collectively, the data show that there was no significant difference between female and male mice in the number of pERK-IR neurons following nonnoxious and noxious CRD. However, female mice did have significantly more pERK-IR neurons in LIII–V than male mice in the no CRD cohorts. $*p < .05$ determined by Kruskal–Wallis test (nonparametric data) with Dunn's multiple comparison tests. Error bars represent the standard error of the mean. (C) Quantitative data gained from dorsal horn sections covering LS spinal cord (S1 spinal levels) comparing the number of pERK-IR neurons per section in each of the dorsal horn subregions (LI–II [dark gray bars], LIII–V [mid-gray bars], DGC [light gray bars], and the SPN [white bars]) following (i) no CRD, (ii) nonnoxious CRD, and (iii) noxious CRD between female (f; pink dots) and male (m; blue dots) mice. Collectively, the data show that there was no significant difference between female and male mice in the number of pERK-IR neurons following no CRD, nonnoxious CRD, and noxious CRD, determined by Kruskal–Wallis test (nonparametric data) with Dunn's multiple comparison tests. Error bars represent the standard error of the mean. (D) Quantitative data gained from caudal medulla DVC cross sections (spanning -7.6 to -7.8 caudal to bregma) comparing the number of pERK-IR neurons per section in the (i) NTS and (ii) DMV following no CRD, nonnoxious CRD, and noxious CRD between female (f; pink dots) and male (m; blue dots) mice. No significant difference in the number of pERK-IR neurons following no CRD, nonnoxious CRD, and noxious CRD was evident between female and male mice, determined by one-way ANOVA (parametric data) with Tukey's multiple comparison tests. Error bars represent the standard error of the mean.

4 | DISCUSSION

This study explored the central neuroanatomy of colorectal vagal and spinal afferent pathways in the mouse. We married anatomical assessment with functionality, by correlating the terminal field distributions of colorectal vagal and spinal afferents with the extent, and distribution, of CRD-activated neurons in the DVC and dorsal horn. We highlight novel aspects of the central neuroanatomy into which spinal and vagal colorectal afferents project, which are relevant to nociceptive and sensory–motor integration. Such comparative assessment of CRD-evoked neuronal activation between VG and DRG, or the DVC and dorsal horn circuits, has never been reported on before. Thus, we expand on the comparative assessment of vagal and spinal colorectal pathways from beyond the knowledge of their peripheral properties and the ganglion distribution of their cell bodies. Furthermore, our findings elucidate differences in the functional anatomy between the vagal and spinal pathways that may mediate their disparate influences on pain-evoked colorectal visceromotor responses.

4.1 | Vagal and dorsal root ganglia

Quantifying labeled neurons within whole CLARITY-cleared ganglia enabled absolute comparisons between the vagal and spinal innervation of the colorectum that has not been captured previously by tissue sections. We showed that colorectal-labeled neurons are most abundant within pelvic DRG, followed by splanchnic DRG (T10–L1) and then VG. Correspondingly, we showed functionally that noxious CRD activates more neurons in the DRG than the VG. Our regional retrograde tracing findings align with previous anatomical and electrophysiological assessments in the mouse, which show vagal afferent innervation is most abundant in the proximal aspects of the colorectum, whereas pelvic afferent innervation is most dense in the distal aspects of the col-

orectum and splanchnic afferent innervation extends relatively evenly along the full length of the colorectum (Brierley et al., 2004; Meerschaert et al., 2020; Osman et al., 2023; Wang et al., 2000). However, given we also assessed terminal field distributions of vagal and spinal afferents from different regions of the colorectum, we were also able to make parallels between the degree of neuronal labeling evident within sensory ganglia and the extent of input within DVC and dorsal horn circuits relevant to nociceptive signaling and sensory–motor integration.

4.2 | Colorectal vagal afferent input into the DVC supporting antinociceptive influences

Corresponding to colorectal-labeled afferent neurons within the VG, we located labeled projections within the caudal medulla DVC. The distribution within NTS subnuclei, the AP and the DMV, was similar to that described in the rat, from the caecum and the descending colon (Altschuler et al., 1991, 1993). Furthermore, the locality of projections within DVC aligns with the area in which central projections of the celiac and accessory celiac branches of the subdiaphragmatic vagus have been localized in rats (Norgren et al., 1988). Our findings provide further evidence of the organ-specific organization of viscerosensory afferent input within NTS subnuclei (Altschuler et al., 1991, 1993; Bassi et al., 2022; Shapiro et al., 1985; Travagli et al., 2006). Moreover, we provide anatomical evidence for colorectal vagal neurons not expressing CGRP, as suggested by recent molecular studies (Matsumoto et al., 2023; Meerschaert et al., 2020). This finding also confirms colorectal-projecting VG neurons are of nodose origin, rather than jugular (Driessen et al., 2015).

Colorectal-labeled fibers in the NTS were primarily from rostral colorectal-injected CTB-647, which aligned with the abundance of VG neurons labeled. However, in the NTS we also observed fibers labeled

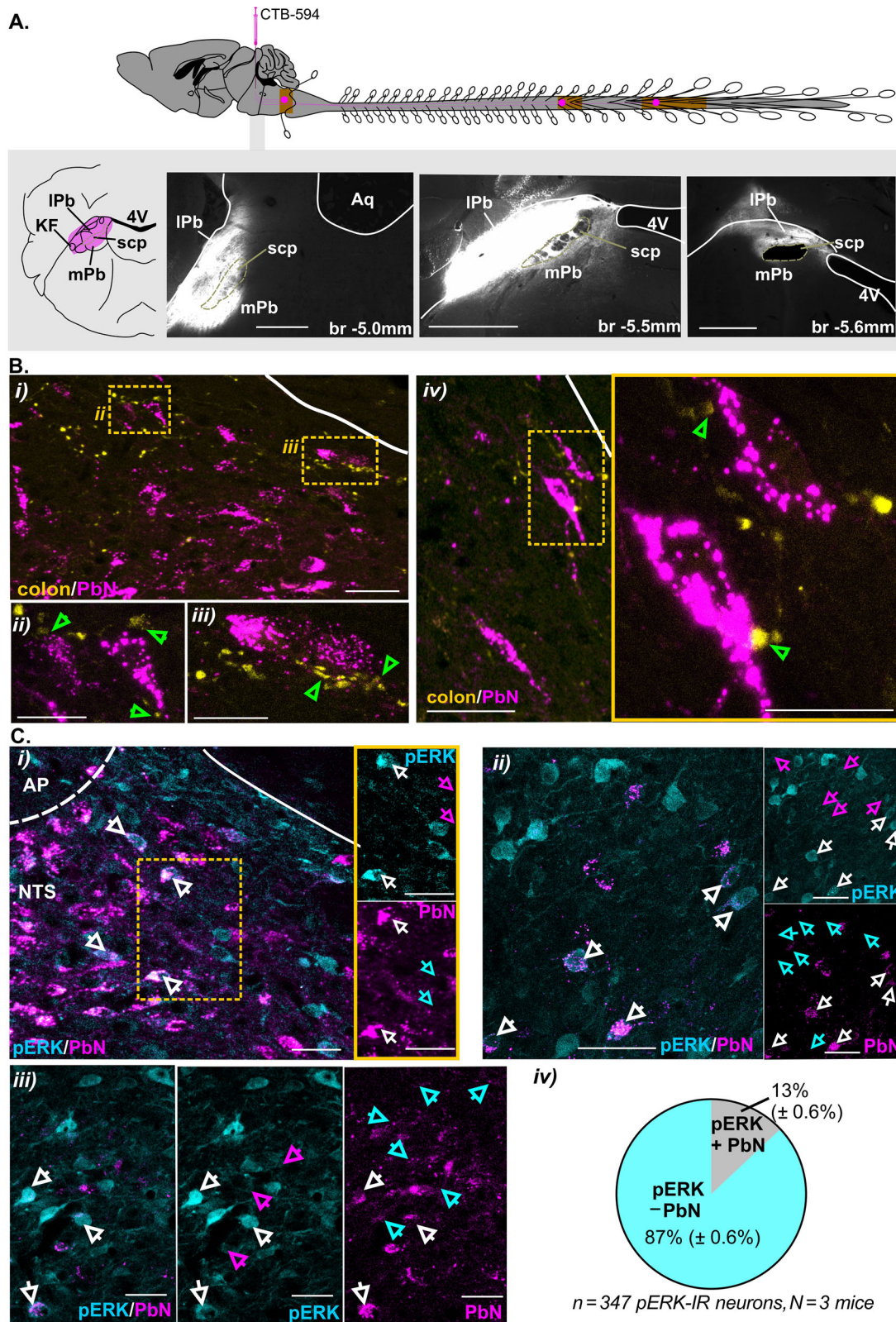


FIGURE 15 Distribution of colorectal retrograde-labeled fibers relative to parabrachial (PbN)-projecting neurons in the nucleus of the solitary tract (NTS). (A) Schematic illustrating the site of tracer CTB-594 (magenta) injection into the pontine PbN complex (magenta-shaded areas) and photomicrographs of brainstem sections (numbers indicate distance from bregma) (Paxinos et al., 2001) showing the spread of injected CTB-594 from one experiment. Scale bars = 100 μ m. Aq, aqueduct; KF, Kölliker–Fuse nucleus; IPb, lateral parabrachial nuclei; mPb, medial parabrachial nuclei; scp, superior cerebellar peduncle; 4V: fourth ventricle. (B) Photomicrographs (i–iv) showing the distribution of

(Continues)

FIGURE 15 (Continued)

colorectal-labeled fibers (yellow) in relation to neurons retrograde-labeled from the PbN (magenta) in the NTS. PbN neurons in apposition to colorectal-labeled fibers are highlighted by green arrows. Images (ii and iii) correspond to regions in (i) within yellow-dotted boxes. (iv) Image in yellow box (scale bar = 10 μm) corresponds to the region within the yellow-dotted box. Scale bars: i and iv = 20 μm ; ii and iii = 10 μm . Photomicrographs are reconstructions from confocal-collected three to four optical sections (1- to 2- μm -thick z-steps). (C) Photomicrographs (i–iii) showing retrograde-labeled PbN neurons (magenta) and pERK-immunoreactive neurons (pERK, cyan) in the NTS following noxious CRD. PbN/pERK-IR neurons are indicated by white arrows. (i) Images in yellow-lined box (scale bar = 10 μm) correspond to the region in the yellow-dotted box. Scale bars = 20 μm . (iv) Quantitative group data showing the mean (\pm standard error of the mean) percentage of pERK-IR neurons within the NTS co-labeled from the PbN (gray region) as a proportion of total pERK-IR neurons following noxious CRD. Data were gained from 4–5 sections/mouse from $N = 3$ male (13 sections in total) mice, in which a total of 42 pERK/PbN neurons were observed in the NTS.

by the most caudal colorectal-injected CTB-488, which did not align with the rarity of CTB-488-labeled neurons in the VG. This potentially reflects the nature of vagal afferent neurons to form complex terminal arborizations within the NTS (Bassi et al., 2022; McGovern et al., 2015). Thus, our findings indicate that the number of VG neurons labeled from distal regions of the colorectum may not directly reflect the amount of information ultimately relayed into the DVC. In agreement, the abundance of pERK-IR neurons in the NTS appeared to contrast with the number of colorectal-labeled VG neurons from any region. Again, this may reflect arborization of vagal terminals activating multiple second-order neurons. Alternatively, spinosolitary projection neurons within the dorsal horn may also contribute to CRD-evoked neuronal activation in the NTS based on a recent mouse study showing that populations of NTS-projecting neurons in the LS dorsal horn are activated by noxious chemical irritants applied to the rectum (Nishida et al., 2022). Conversely, studies using vagal denervation clearly show that direct vagal afferent input chiefly contributes to NTS neuronal activation evoked by proximal colon distension (Monnikes et al., 2003).

Functional studies show that visceromotor responses evoked by CRD, at nonnoxious and noxious ranges, are enhanced by subdiaphragmatic vagotomy (Chen et al., 2008; Gschossmann et al., 2002). Mediating this, it has been proposed that colorectal vagal afferents recruit centralized circuits with opioidergic descending outputs to the spinal cord (Gschossmann et al., 2002). We found that a small population of NTS neurons activated by noxious CRD project to the PbN, which may facilitate the recruitment of descending pain modulation circuits. Furthermore, we also observed colorectal vagal projections in apposition to NTS neurons that were immunoreactive for TH. This finding aligns with a study in rat, showing that just under half of the NTS neurons activated by distension of the proximal colon are catecholaminergic (Wang et al., 2009). As such, our findings provide anatomical evidence for colorectal vagal input directly recruiting catecholaminergic NTS neurons similarly to vagal afferents from the stomach and the small intestine (Appleyard et al., 2007; Bassi et al., 2022). Given that catecholaminergic NTS neurons projecting to the periaqueductal gray have been implicated in the modulation of gastric nociceptive signaling (Chen et al., 1995), our findings potentially identify elements of the central anatomy relevant to supporting vagal antinociceptive influences on colorectal visceromotor responses.

4.3 | Colorectal spinal afferent input in the dorsal horn supporting nociceptive signaling

Aligning with the abundance of colorectal-labeled neurons observed in the pelvic DRG, in particular from the most caudal injection sites, labeled projections were dense within the dorsal horn at the L6–S1 spinal cord. The relative sparsity of labeled projections in the TL spinal cord paralleled observations in the splanchnic DRG (T12–L1 DRG). However, unlike the even distribution of TL DRG neurons labeled from different colorectal regions, within the TL spinal cord, projections were predominantly labeled from caudally directed injections. Differences in the density of colorectal retrograde labeling between the TL and LS dorsal horn were reflected in the amount of neuronal activation evoked by CRD. The overall number of CRD-activated neurons were greater in the LS dorsal horn than in the TL dorsal horn. This confirms our previous findings in mice (Harrington et al., 2019) and others in rats (Traub, 2000; Traub et al., 1992, 1993). Collectively, the differences between the TL and LS spinal cord in the number of CRD-activated neurons align with findings from mice studies comparing the mechanosensory activation thresholds of splanchnic and pelvic colorectal afferent endings (Brierley et al., 2004; Feng et al., 2011; Hughes et al., 2009). These studies show that the vast majority of splanchnic afferent endings, which relay into the TL spinal cord, have high thresholds to mechanical stimuli (i.e., high-threshold nociceptive afferent endings). In contrast, pelvic afferent endings, which relay into the LS spinal cord, have heterogeneous activation thresholds to mechanical stimuli and are activated by circumferential stretch at innocuous or noxious pressures, or both.

Expanding on these previous studies, comparisons of neuronal activation occurred in the dorsal horn between nonnoxious and noxious CRD, and between spinal cord levels, providing new insight into the spinal afferent input and dorsal horn circuits recruited to colorectal nociceptive processing. In the TL dorsal horn, nonnoxious CRD did not evoke neuronal activation over that of no CRD controls. However, noxious CRD evoked significant activation within dorsal horn regions relevant to nociceptive processing, such as LI and LV. Conversely, in the LS dorsal horn, nonnoxious CRD activated neurons above that of no CRD throughout LI–LV and the SPN. On the other hand, neuronal activation specifically evoked by noxious CRD occurred within the DGC. These findings align with our previous study showing that CRD activates a network of excitatory and inhibitory interneurons within LI–III of the LS dorsal horn, but not the TL dorsal horn (Harrington et al.,

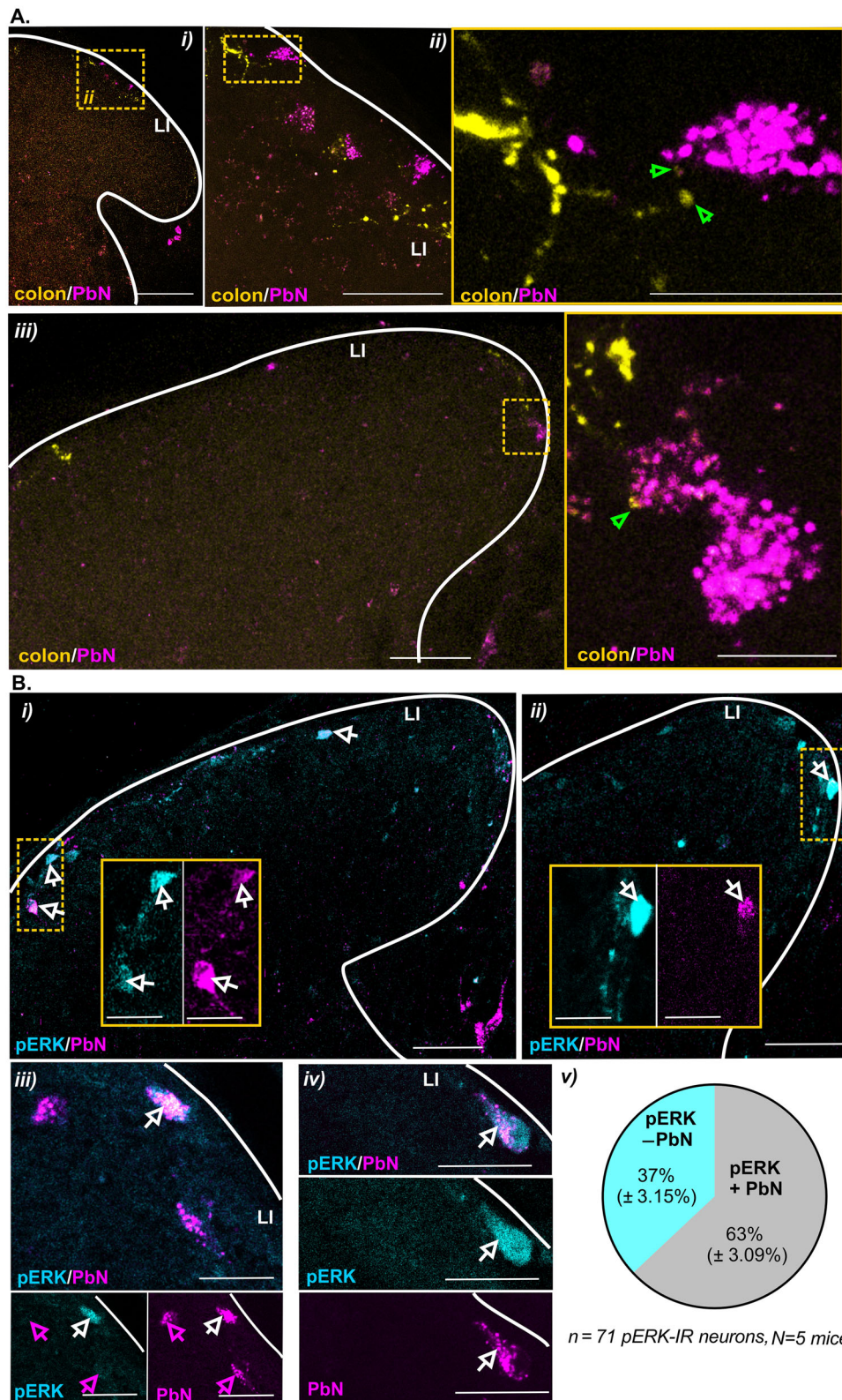


FIGURE 16 Distribution of colorectal retrograde-labeled fibers relative to parabrachial (PbN)-projecting neurons in the thoracolumbar spinal cord dorsal horn. (A) Photomicrographs (i–iii) showing the distribution of colorectal retrograde-labeled fibers (yellow) in relation to neurons retrogradely labeled from the PbN (magenta) in dorsal horn lamina I (LI) at the thoracolumbar level of the spinal cord. PbN neurons in apposition to colorectal-labeled fibers are highlighted by green arrows. Image (ii) is a higher magnification of the region within the yellow dotted box in (i). Images in (ii) and (iii) in yellow-lined box (scale bar = 10 μm) correspond to the region within yellow-dotted boxes. Scale bars = i and iii = 50 μm ;

(Continues)

FIGURE 16 (Continued)

ii = 20 μ m. Photomicrographs are reconstructions from confocal-collected three to four optical sections (1- to 2- μ m-thick z-steps). (B) Photomicrographs (i–iv) showing retrograde-labeled PbN neurons (magenta) and pERK-immunoreactive neurons (pERK, cyan) in LI following noxious CRD. PbN/pERK-IR neurons are indicated by white arrows. Inset images in (i) and (ii) are a higher magnification of regions within the yellow-dotted boxes. Scale bars: i and ii = 50 μ m (inset 20 μ m); iii and iv = 20 μ m. (v) Quantitative group data showing the mean (\pm standard error of the mean) percentage of pERK-IR neurons within LI co-labeled from the PbN (gray region) as a proportion of total pERK-IR neurons within LI following noxious CRD. Spinal cord data were gained from 2–6 sections/mouse from $N = 5$ male mice (22 sections in total), in which a total of 42 pERK/PbN neurons were observed.

2019). Expanding on these findings, in this current study, we show that splanchnic and pelvic colorectal afferents differentially recruit dorsal horn LI neurons to the ascending relay of colorectal nociceptive transmission into the pontine PbN. The spatial relationship we reported between colorectal afferent projections in LI of the TL dorsal horn and PbN-projecting neurons—moreover, the large proportion of CRD-activated neurons in TL dorsal horn LI projecting to the PbN—aligns with colorectal splanchnic afferents directly recruiting putative LI nociceptive circuits. Conversely, we observed a minor population of LS dorsal horn neurons in LI activated by CRD projecting to the PbN. Collectively, these findings provide further anatomical evidence for colorectal pelvic afferents recruiting a more heterogeneous population of dorsal horn neurons than that of splanchnic afferents, which are not solely concerned with nociceptive transmission (Al-Chaer et al., 1996; Nakamori et al., 2018; Ness et al., 1989; Nishida et al., 2022).

As the PbN is known to have a role in recruiting descending inhibitory circuits, it warrants further investigation if PbN-projecting neurons, in either the TL and LS spinal cord or both, do indeed facilitate colorectal nociception or act to recruit descending feedback. This is particularly relevant, given that functional studies show colorectal nociceptive transmission through the spinal cord is regulated by tonic descending inhibition (Ness et al., 1987, 1989). Moreover, there is evidence for the spino-PbN pathway recruiting descending opioidergic inhibition of CRD-evoked neuronal activation in the LS dorsal horn (Murphy et al., 2009). Studies in rats show that noxious CRD activates greater numbers of PbN-projecting neurons in the LS dorsal horn than in the TL dorsal horn (Traub et al., 2002). Unlike our findings, these PbN-projecting neurons are present within lateral and medial gray matter and the SPN, in addition to LI (Murphy et al., 2009; Traub et al., 2002). Interestingly, a recent optogenetic study in mice showed that populations of sacral dorsal horn PbN-projecting neurons within the DGC and lateral gray matter, which express VGlut3, are involved in aversion rather than nociceptive aspects of colorectal inflammation-evoked visceromotor responses (Qi et al., 2023). However, we did not observe pERK-IR PbN-projecting neurons within the DGC, nor the SPN, despite their proximity of colorectal projections. Such discrepancies may reflect species differences, variability in CRD balloon location (rectal vs. colorectal), intensity and length of stimulation, or PbN tracing rostral–caudal location. Differences may also be due to the neuronal activation marker used (pERK vs. cFos), given that activation markers are proposed to be selective for populations of neurons influenced by the type of afferent input they receive (Polgar et al., 2013).

4.3.1 | Sites of sensory afferent integration into efferent motor circuits

The dorsal horn and the NTS are also sites where colorectal afferent information is integrated into autonomic nuclei to shape affective defecation responses. We observed retrograde-labeled fibers projecting within the SPN, which is known to contain parasympathetic preganglionic motor neurons. This finding aligns with those from studies in rats that used tracing from isolated pelvic nerves (Mawe et al., 1986; Morgan et al., 1981; Nadelhaft et al., 1984) and illustrates the anatomy supporting pelvic afferent facilitation of colonic motility reflexes and defecation independent of spinobulbar circuits (de Groat et al., 1981; Smith-Edwards et al., 2019). We also observed colorectal-labeled fibers within the DMV, which is known to contain parasympathetic dorsal vagal motor neurons. We found that colorectal-labeled fibers in the DMV showed similar density and morphology as those from the stomach, small intestine, heart, and trachea (Bassi et al., 2022). Collectively, these findings align with the SPN and DMV being sites of sensory–motor integration. However, we did not observe a link between CRD intensity and evoked neuronal activation in the SPN and DMV, unlike the superficial dorsal horn and the DGC. This may indicate that afferent input targeting the SPN and DMV primarily mediates affective defecation reflexes, rather than urgency as stimuli intensify. We also observed retrograde-labeled cell bodies within the DMV and SPN, not all of which were pERK-IR following noxious CRD. As CTB does not jump synapses, labeling of these cell bodies has been proposed to be via efferent endings located in the colon wall. In accordance, projections of DMV neurons have been located with the myenteric ganglia along the length of the mouse colon (Tao et al., 2021). As for SPN neurons, tracer injections may have occurred within small microganglia localized in the rectal adventitia that are known to contain populations of rectospinal neurons (Fuller-Jackson et al., 2021; Luckensmeyer et al., 1998; Olsson et al., 2006). This aligns with observing SPN neurons being labeled solely from caudal CTB injections, whereas DMV neurons were labeled from all injection sites.

Collectively, this study provides new information on the central aspects of the sensory afferent axis shaping colorectal visceromotor responses. Importantly, these findings serve as an anatomical framework to guide and interpret further exploration of the central circuits into which vagal and spinal afferent pathways relay to mediate colorectal pain. Moreover, such information will aid in identifying novel sites of neural remodeling in mouse models of chronic visceral pain and sensory–motor dysfunction.

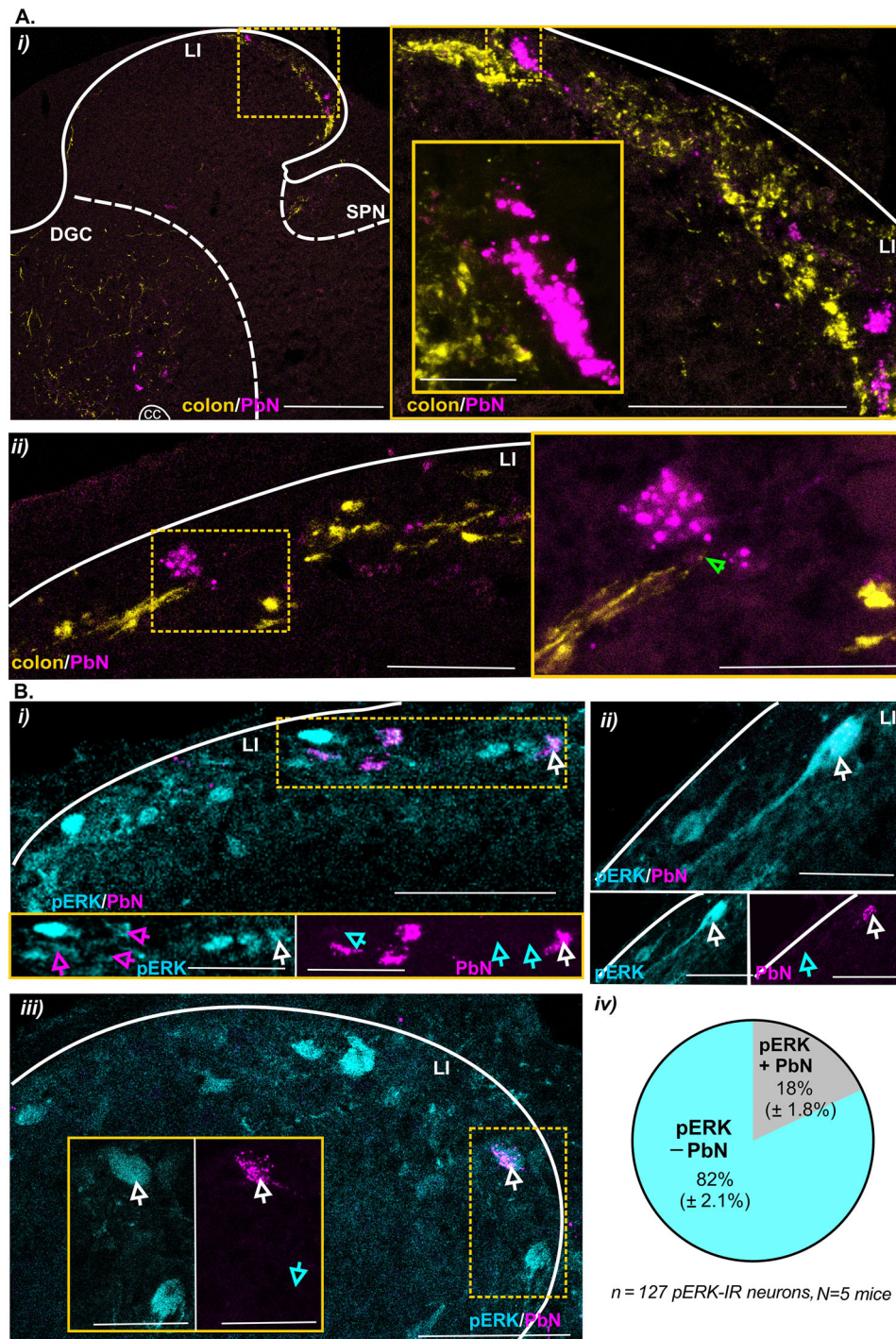


FIGURE 17 Distribution of colorectal retrograde-labeled fibers relative to parabrachial (PbN)-projecting neurons in the lumbosacral spinal cord dorsal horn. (A) Photomicrographs (i and ii) showing the distribution of colorectal-labeled fibers (yellow) in relation to neurons retrograde-labeled from the PbN (magenta) in the dorsal horn at the sacral level of the spinal cord. PbN neurons in apposition to colorectal-labeled fibers are highlighted by green arrows. (i) Yellow-lined boxed image (scale bar = 50 μ m, inset image scale bar = 5 μ m) corresponds to the region within the yellow-dotted box in the lower magnification image (scale bar = 100 μ m). (ii) Image in yellow-lined box (scale bar = 10 μ m) corresponds to the region within the yellow-dotted box in the lower magnification image (scale bar = 20 μ m). (B) Photomicrographs (i–iii) showing retrograde-labeled PbN neurons (magenta) and pERK-immunoreactive neurons (pERK, cyan) in lamina I (LI) following noxious CRD. PbN/pERK-IR neurons are indicated by white arrows. Inset images in (i) and (iii) correspond to regions within the yellow-dotted boxes in their respective low-magnification image. Photomicrographs are reconstructions from confocal-collected three to four optical sections (1- to 2- μ m-thick z-steps). Scale bars: i and iii = 50 μ m (insets i and iii = 25 μ m); ii = 20 μ m. (iv) Quantitative group data showing the mean (\pm standard error of the mean) percentage of pERK-IR neurons within LI co-labeled from the PbN (gray region) as a proportion of total pERK-IR neurons within LI following noxious CRD. Data gained from 2–6 sections/mouse from *N* = 5 male mice (22 sections), in which a total of 19 pERK/PbN neurons were observed. Dashed lines indicate the lateral borders of the DGC (dorsal gray commissure) and the SPN (sacral parasympathetic nuclei). cc, central canal.

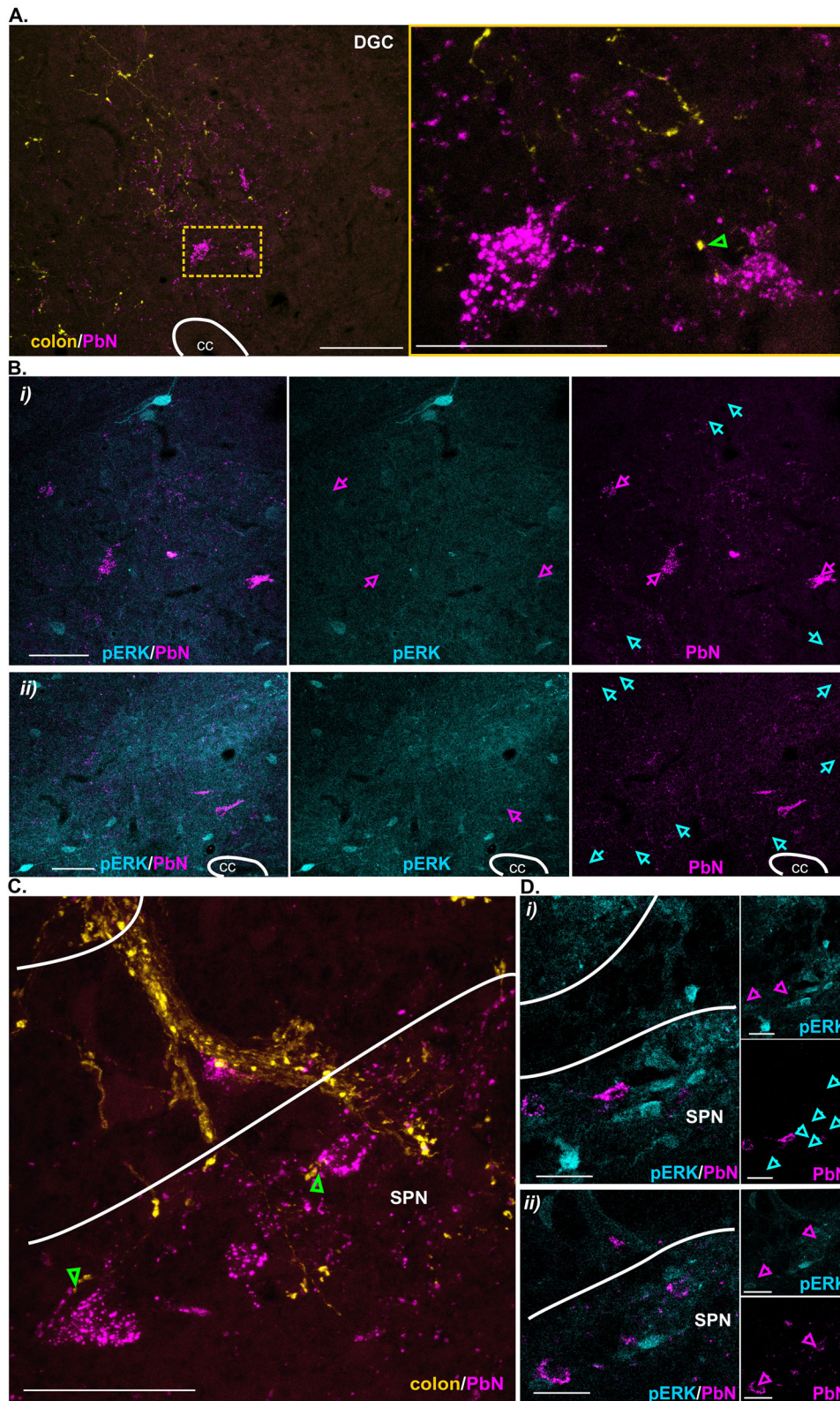


FIGURE 18 Distribution of colorectal retrograde-labeled fibers in the lumbo-sacral spinal cord dorsal horn dorsal gray commissure (DGC) and sacral parasympathetic nuclei (SPN) relative to parabrachial (PbN)-projecting neurons. (A) Photomicrograph showing the distribution of colorectal retrograde-labeled fibers (yellow) in relation to neurons retrogradely labeled from the PbN (magenta) in the dorsal horn dorsal gray commissure (DGC) at the sacral level of the spinal cord. PbN neurons in apposition to colorectal-labeled fibers are highlighted by green arrows. (i) Yellow-boxed image (scale bar = 10 μ m) corresponds to the yellow-dotted box region in the low-magnification image (scale bar = 50 μ m). (B) Photomicrographs (i and ii) showing retrograde-labeled PbN neurons (magenta) and phosphorylated MAP ERK1/2 kinase (pERK)-immunoreactive neurons (cyan) in the

(Continues)

FIGURE 18 (Continued)

DGC following in vivo noxious colorectal distension (CRD). PbN neurons are indicated by magenta arrows and pERK-IR neurons are indicated by cyan arrows. Scale bars = 50 μm . (C) Photomicrograph showing the distribution of colorectal-labeled fibers (yellow) in relation to neurons retrogradely labeled from the PbN (magenta) in the dorsal horn sacral parasympathetic nuclei (SPN) at the sacral level of the spinal cord. PbN neurons in apposition to colorectal-labeled fibers are highlighted by green arrows. Scale bar = 20 μm . (D) Photomicrographs (i and ii) showing retrograde-labeled PbN neurons (magenta) and phosphorylated MAP ERK1/2 kinase (pERK)-immunoreactive neurons (cyan) in the SPN following in vivo noxious colorectal distension (CRD). PbN neurons are indicated by magenta arrows and pERK-IR neurons are indicated by cyan arrows. Scale bars = 20 μm .

AUTHOR CONTRIBUTIONS

Andrea M. Harrington, Alice E. McGovern, Stuart B. Mazzone, and Stuart M. Brierley devised experiments. Andrea M. Harrington, QingQing Wang, and Sonia Garcia Caraballo performed experiments and analyzed the data. Andrea M. Harrington prepared figures and wrote the manuscript. Stuart M. Brierley, Stuart B. Mazzone, Alice E. McGovern, and Grigori Rychkov provided scientific input and corrections to the manuscript.

ACKNOWLEDGMENTS

The authors acknowledge Adelaide Microscopy and the South Australian Health and Medical Research Institute (SAHMRI) for the provision of microscopy infrastructure.

CONFLICT OF INTEREST STATEMENT

The authors declare no conflicts of interest.

DATA AVAILABILITY STATEMENT

The data that support the findings of this study are openly available in Flinders University Repository of Open Access Data Sets at <https://doi.org/10.25451/flinders.19130702.v1>. Microscopy images that support the findings of this study are available from the corresponding author upon reasonable request.

ORCID

Grigori Rychkov  <https://orcid.org/0000-0002-2788-2977>

Andrea M. Harrington  <https://orcid.org/0000-0002-1562-4137>

PEER REVIEW

The peer review history for this article is available at <https://publons.com/publon/10.1002/cne.25546>

REFERENCES

- Al-Chaer, E. D., Lawand, N. B., Westlund, K. N., & Willis, W. D. (1996). Pelvic visceral input into the nucleus gracilis is largely mediated by the postsynaptic dorsal column pathway. *Journal of Neurophysiology*, 76(4), 2675–2690. <https://doi.org/10.1152/jn.1996.76.4.2675>
- Altschuler, S. M., Escardo, J., Lynn, R. B., & Miselis, R. R. (1993). The central organization of the vagus nerve innervating the colon of the rat. *Gastroenterology*, 104(2), 502–509. [https://doi.org/10.1016/0016-5085\(93\)90419-D](https://doi.org/10.1016/0016-5085(93)90419-D)
- Altschuler, S. M., Ferenci, D. A., Lynn, R. B., & Miselis, R. R. (1991). Representation of the cecum in the lateral dorsal motor nucleus of the vagus nerve and commissural subnucleus of the nucleus tractus solitarii in rat. *Journal of Comparative Neurology*, 304(2), 261–274. <https://doi.org/10.1002/cne.903040209>
- Appleyard, S. M., Marks, D., Kobayashi, K., Okano, H., Low, M. J., & Andresen, M. C. (2007). Visceral afferents directly activate catecholamine neurons in the solitary tract nucleus. *Journal of Neuroscience*, 27(48), 13292–13302. <https://doi.org/10.1523/JNEUROSCI.3502-07.2007>
- Bankhead, P., Loughrey, M. B., Fernández, J. A., Dombrowski, Y., Mcart, D. G., Dunne, P. D., Mcquaid, S., Gray, R. T., Murray, L. J., Coleman, H. G., James, J. A., Salto-Tellez, M., & Hamilton, P. W. (2017). QuPath: Open source software for digital pathology image analysis. *Scientific Reports*, 7(1), 16878. <https://doi.org/10.1038/s41598-017-17204-5>
- Bassi, J. K., Connelly, A. A., Butler, A. G., Liu, Y., Ghanbari, A., Farmer, D. G. S., Jenkins, M. W., Melo, M. R., Mcdougall, S. J., & Allen, A. M. (2022). Analysis of the distribution of vagal afferent projections from different peripheral organs to the nucleus of the solitary tract in rats. *Journal of Comparative Neurology*, 530(17), 3072–3103. <https://doi.org/10.1002/cne.25398>
- Brierley, S. M., Jones, R. C. W., Gebhart, G. F., & Blackshaw, L. A. (2004). Splanchnic and pelvic mechanosensory afferents signal different qualities of colonic stimuli in mice. *Gastroenterology*, 127, 166–178. <https://doi.org/10.1053/j.gastro.2004.04.008>
- Cameron, D., Polgár, E., Gutierrez-Mecinas, M., Gomez-Lima, M., Watanabe, M., & Todd, A. J. (2015). The organisation of spinoparabrachial neurons in the mouse. *Pain*, 156(10), 2061–2071. <https://doi.org/10.1097/j.pain.0000000000000270>
- Castro, J., Harrington, A. M., Garcia-Caraballo, S., Maddern, J., Grundy, L., Zhang, J., Page, G., Miller, P. E., Craik, D. J., Adams, D. J., & Brierley, S. M. (2017). α -Conotoxin Vc1.1 inhibits human dorsal root ganglion neuroexcitability and mouse colonic nociception via GABAB receptors. *Gut*, 66(6), 1083–1094. <https://doi.org/10.1136/gutjnl-2015-310971>
- Castro, J., Harrington, A. M., Hughes, P. A., Martin, C. M., Ge, P., Shea, C. M., Jin, H., Jacobson, S., Hannig, G., Mann, E., Cohen, M. B., Maccougall, J. E., Lavins, B. J., Kurtz, C. B., Silos-Santiago, I., Johnston, J. M., Currie, M. G., Blackshaw, L. A., & Brierley, S. M. (2013). Linaclotide inhibits colonic nociceptors and relieves abdominal pain via guanylate cyclase-C and extracellular cyclic guanosine 3',5'-monophosphate. *Gastroenterology*, 145(6), 1334.e11–1346.e11. <https://doi.org/10.1053/j.gastro.2013.08.017>
- Castro, J., Maddern, J., Erickson, A., Caldwell, A., Grundy, L., Harrington, A. M., & Brierley, S. M. (2021). Pharmacological modulation of voltage-gated sodium (NaV) channels alters nociception arising from the female reproductive tract. *Pain*, 162(1), 227–242. <https://doi.org/10.1097/j.pain.0000000000002036>
- Chen, L.-W., Rao, Z.-R., & Shi, J.-W. (1995). Catecholaminergic neurons in the nucleus tractus solitarii which send their axons to the midbrain periaqueductal gray express Fos protein after noxious stimulation of the stomach: A triple labeling study in the rat. *Neuroscience Letters*, 189(3), 179–181. [https://doi.org/10.1016/0304-3940\(95\)11475-C](https://doi.org/10.1016/0304-3940(95)11475-C)
- Chen, S. L., Wu, X. Y., Cao, Z. J., Fan, J., Wang, M., Owyang, C., & Li, Y. (2008). Subdiaphragmatic vagal afferent nerves modulate visceral pain. *American Journal of Physiology—Gastrointestinal and Liver Physiology*, 294(6), G1441–G1449. <https://doi.org/10.1152/ajpgi.00588.2007>
- Christianson, J. A., & Gebhart, G. F. (2007). Assessment of colon sensitivity by luminal distension in mice. *Nature Protocols*, 2(10), 2624–2631. <https://doi.org/10.1038/nprot.2007.392>
- De Araujo, A. D., Mobli, M., Castro, J., Harrington, A. M., Vetter, I., Dekan, Z., Muttenthaler, M., Wan, J., Lewis, R. J., King, G. F., Brierley, S. M.,

- & Alewood, P. F. (2014). Selenoether oxytocin analogues have analgesic properties in a mouse model of chronic abdominal pain. *Nature Communications*, 5, 3165. <https://doi.org/10.1038/ncomms4165>
- De Groat, W. C., Nadelhaft, I., Milne, R. J., Booth, A. M., Morgan, C., & Thor, K. (1981). Organization of the sacral parasympathetic reflex pathways to the urinary bladder and large intestine. *Journal of the Autonomic Nervous System*, 3(2-4), 135–160. [https://doi.org/10.1016/0165-1838\(81\)90059-X](https://doi.org/10.1016/0165-1838(81)90059-X)
- Driessen, A. K., Farrell, M. J., Mazzone, S. B., & McGovern, A. E. (2015). The role of the paratrigeminal nucleus in vagal afferent evoked respiratory reflexes: A neuroanatomical and functional study in guinea pigs. *Frontiers in Physiology*, 6, 378. <https://doi.org/10.3389/fphys.2015.00378>
- Feng, B., & Gebhart, G. F. (2011). Characterization of silent afferents in the pelvic and splanchnic innervations of the mouse colorectum. *American Journal of Physiology—Gastrointestinal and Liver Physiology*, 300(1), G170–G180. <https://doi.org/10.1152/ajpgi.00406.2010>
- Fuller-Jackson, J. P., Osborne, P. B., & Keast, J. R. (2021). Regional targeting of bladder and urethra afferents in the lumbosacral spinal cord of male and female rats: A multiscale analysis. *eNeuro*, 8(6), Article ENEURO.0364–21.2021. <https://doi.org/10.1523/ENEURO.0364-21.2021>
- Ge, P., Ren, J., Harrington, A. M., Grundy, L., Castro, J., Brierley, S. M., & Hannig, G. (2019). Linaclotide treatment reduces endometriosis-associated vaginal hyperalgesia and mechanical allodynia through viscerovisceral cross-talk. *Pain*, 160(11), 2566–2579. <https://doi.org/10.1097/j.pain.0000000000001657>
- Gotts, J., Atkinson, L., Yanagawa, Y., Deuchars, J., & Deuchars, S. A. (2016). Co-expression of GAD67 and choline acetyltransferase in neurons in the mouse spinal cord: A focus on lamina X. *Brain Research*, 1646, 570–579. <https://doi.org/10.1016/j.brainres.2016.07.001>
- Grundy, L., Caldwell, A., Garcia Caraballo, S., Erickson, A., Schober, G., Castro, J., Harrington, A. M., & Brierley, S. M. (2020). Histamine induces peripheral and central hypersensitivity to bladder distension via the histamine H1 receptor and TRPV1. *American Journal of Physiology—Renal Physiology*, 318(2), F298–F314. <https://doi.org/10.1152/ajprenal.00435.2019>
- Grundy, L., Caldwell, A., Garcia-Caraballo, S., Grundy, D., Spencer, N. J., Dong, X., Castro, J., Harrington, A. M., & Brierley, S. M. (2021). Activation of MrgprA3 and MrgprC11 on bladder-innervating afferents induces peripheral and central hypersensitivity to bladder distension. *Journal of Neuroscience*, 41(17), 3900–3916. <https://doi.org/10.1523/JNEUROSCI.0033-21.2021>
- Grundy, L., Harrington, A. M., Caldwell, A., Castro, J., Staikopoulos, V., Zagorodnyuk, V. P., Brookes, S. J. H., Spencer, N. J., & Brierley, S. M. (2019). Translating peripheral bladder afferent mechanosensitivity to neuronal activation within the lumbosacral spinal cord of mice. *Pain*, 160(4), 793–804. <https://doi.org/10.1097/j.pain.0000000000001453>
- Grundy, L., Harrington, A. M., Castro, J., Garcia-Caraballo, S., Deiteren, A., Maddern, J., Rychkov, G. Y., Ge, P., Peters, S., Feil, R., Miller, P., Ghetti, A., Hannig, G., Kurtz, C. B., Silos-Santiago, I., & Brierley, S. M. (2018). Chronic linaclotide treatment reduces colitis-induced neuroplasticity and reverses persistent bladder dysfunction. *JCI Insight*, 3(19), e121841. <https://doi.org/10.1172/jci.insight.121841>
- Gschossmann, J. M., Mayer, E. A., Miller, J. C., & Raybould, H. E. (2002). Subdiaphragmatic vagal afferent innervation in activation of an opioidergic antinociceptive system in response to colorectal distension in rats. *Neurogastroenterology and Motility*, 14(4), 403–408. <https://doi.org/10.1046/j.1365-2982.2002.00345.x>
- Harrington, A. M. (2023). Translating colonic sensory afferent peripheral mechanosensitivity into the spinal cord dorsal horn. In S. M. Brierley & N. J. Spencer (Eds.), *Visceral pain* (pp. 161–181) Springer.
- Harrington, A. M., Brierley, S. M., Isaacs, N., Hughes, P. A., Castro, J., & Blackshaw, L. A. (2012). Sprouting of colonic afferent central terminals and increased spinal mitogen-activated protein kinase expression in a mouse model of chronic visceral hypersensitivity. *Journal of Comparative Neurology*, 520(10), 2241–2255. <https://doi.org/10.1002/cne.23042>
- Harrington, A. M., Brierley, S. M., Isaacs, N. J., Young, R. L., & Ashley Blackshaw, L. (2013). Identifying spinal sensory pathways activated by noxious esophageal acid. *Neurogastroenterology and Motility*, 25(10), e660–e668. <https://doi.org/10.1111/nmo.12180>
- Harrington, A. M., Caraballo, S. G., Maddern, J. E., Grundy, L., Castro, J., & Brierley, S. M. (2019). Colonic afferent input and dorsal horn neuron activation differs between the thoracolumbar and lumbosacral spinal cord. *American Journal of Physiology—Gastrointestinal and Liver Physiology*, 317(3), G285–G303. <https://doi.org/10.1152/ajpgi.00013.2019>
- Harrington, A. M., Castro, J., Erickson, A., Grundy, L., & Brierley, S. M. (2018). Extrinsic sensory afferent nerves innervating the gastrointestinal tract in health and disease. In H. M. Said (Ed.), *Physiology of the gastrointestinal tract* (6th ed., pp. 387–418). Academic Press.
- Herrity, A. N., Rau, K. K., Petruska, J. C., Stirling, D. P., & Hubscher, C. H. (2014). Identification of bladder and colon afferents in the nodose ganglia of male rats. *Journal of Comparative Neurology*, 522(16), 3667–3682. <https://doi.org/10.1002/cne.23629>
- Huffman, W. J., Subramanian, S., Rodriguiz, R. M., Wetsel, W. C., Grill, W. M., & Terrando, N. (2019). Modulation of neuroinflammation and memory dysfunction using percutaneous vagus nerve stimulation in mice. *Brain Stimulation*, 12(1), 19–29. <https://doi.org/10.1016/j.brs.2018.10.005>
- Hughes, P. A., Brierley, S. M., Martin, C. M., Brookes, S. J. H., Linden, D. R., & Blackshaw, L. A. (2009). Post-inflammatory colonic afferent sensitization: Different subtypes, different pathways, and different time-courses. *Gut*, 58(10), 1333–1341. <https://doi.org/10.1136/gut.2008.170811>
- Hwang, S. J., Burette, A., & Valtchanoff, J. G. (2003). VR1-positive primary afferents contact NK1-positive spinoparabrachial neurons. *Journal of Comparative Neurology*, 460(2), 255–265. <https://doi.org/10.1002/cne.10647>
- Katter, J. T., Dado, R. J., Kostarczyk, E., & Giesler, G. J. jr (1996). Spinothalamic and spinohypothalamic tract neurons in the sacral spinal cord of rats. I. Locations of antidromically identified axons in the cervical cord and diencephalon. *Journal of Neurophysiology*, 75(6), 2581–2605. <https://doi.org/10.1152/jn.1996.75.6.2581>
- Kyloh, M. A., Hibberd, T. J., Castro, J., Harrington, A. M., Travis, L., Dodds, K. N., Wiklendt, L., Brierley, S. M., Zagorodnyuk, V. P., & Spencer, N. J. (2022). Disengaging spinal afferent nerve communication with the brain in live mice. *Communications Biology*, 5(1), 915. <https://doi.org/10.1038/s42003-022-03876-x>
- Lein, E. S., Hawrylycz, M. J., Ao, N., Ayres, M., Bensinger, A., Bernard, A., Boe, A. F., Boguski, M. S., Brockway, K. S., Byrnes, E. J., Chen, L., Chen, L., Chen, T.-M., Chi Chin, M., Chong, J., Crook, B. E., Czaplinska, A., Dang, C. N., Datta, S., ... Jones, A. R. (2007). Genome-wide atlas of gene expression in the adult mouse brain. *Nature*, 445(7124), 168–176. <https://doi.org/10.1038/nature05453>
- Luckensmeyer, G. B., & Keast, J. R. (1998). Characterisation of the adventitial rectal ganglia in the male rat by their immunohistochemical features and projections. *Journal of Comparative Neurology*, 396(4), 429–441. [https://doi.org/10.1002/\(SICI\)1096-9861\(19980713\)396:4%3c429::AID-CNE2%3e3.0.CO;2-3](https://doi.org/10.1002/(SICI)1096-9861(19980713)396:4%3c429::AID-CNE2%3e3.0.CO;2-3)
- Matsumoto, K., Sugimoto, F., Mizuno, T., Hayashi, T., Okamura, R., Nishioka, T., Yasuda, H., Horie, S., Kido, M. A., & Kato, S. (2023). Immunohistochemical characterization of transient receptor potential vanilloid types 2 and 1 in a trinitrobenzene sulfonic acid-induced rat colitis model with visceral hypersensitivity. *Cell and Tissue Research*, 391(2), 287–303. <https://doi.org/10.1007/s00441-022-03723-9>
- Mawe, G. M., Bresnahan, J. C., & Beattie, M. S. (1986). A light and electron microscopic analysis of the sacral parasympathetic nucleus after labelling primary afferent and efferent elements with HRP. *Journal of Comparative Neurology*, 250(1), 33–57. <https://doi.org/10.1002/cne.902500104>
- McGovern, A. E., Davis-Poynter, N., Yang, S.-K., Simmons, D. G., Farrell, M. J., & Mazzone, S. B. (2015). Evidence for multiple sensory circuits in the

- brain arising from the respiratory system: An anterograde viral tract tracing study in rodents. *Brain Structure and Function*, 220(6), 3683–3699. <https://doi.org/10.1007/s00429-014-0883-9>
- McGovern, A. E., & Mazzone, S. B. (2010). Characterization of the vagal motor neurons projecting to the Guinea pig airways and esophagus. *Frontiers in Neurology*, 1, 153. <https://doi.org/10.3389/fneur.2010.00153>
- Meerschaert, K. A., Adelman, P. C., Friedman, R. L., Albers, K. M., Koerber, H. R., & Davis, B. M. (2020). Unique molecular characteristics of visceral afferents arising from different levels of the neuraxis: Location of afferent somata predicts function and stimulus detection modalities. *Journal of Neuroscience*, 40(38), 7216–7228. <https://doi.org/10.1523/JNEUROSCI.1426-20.2020>
- Miyaji, M., Kortum, R. L., Surana, R., Li, W., Woolard, K. D., Simpson, R. M., Samelson, L. E., & Sommers, C. L. (2009). Genetic evidence for the role of Erk activation in a lymphoproliferative disease of mice. *Proceedings of the National Academy of Sciences of the United States of America*, 106(34), 14502–14507. <https://doi.org/10.1073/pnas.0903894106>
- Mönnikes, H., Rüter, J., König, M., Grote, C., Kobelt, P., Klapp, B. F., Arnold, R., Wiedenmann, B., & Tebbe, J. J. (2003). Differential induction of c-fos expression in brain nuclei by noxious and non-noxious colonic distension: Role of afferent C-fibers and 5-HT3 receptors. *Brain Research*, 966(2), 253–264. [https://doi.org/10.1016/S0006-8993\(02\)04197-5](https://doi.org/10.1016/S0006-8993(02)04197-5)
- Morgan, C., Nadelhaft, I., & De Groat, W. C. (1981). The distribution of visceral primary afferents from the pelvic nerve to Lissauer's tract and the spinal gray matter and its relationship to the sacral parasympathetic nucleus. *Journal of Comparative Neurology*, 201(3), 415–440. <https://doi.org/10.1002/cne.902010308>
- Murphy, A. Z., Suckow, S. K., Johns, M., & Traub, R. J. (2009). Sex differences in the activation of the spinoparabrachial circuit by visceral pain. *Physiology and Behavior*, 97(2), 205–212. <https://doi.org/10.1016/j.physbeh.2009.02.037>
- Nadelhaft, I., & Booth, A. M. (1984). The location and morphology of preganglionic neurons and the distribution of visceral afferents from the rat pelvic nerve: A horseradish peroxidase study. *Journal of Comparative Neurology*, 226(2), 238–245. <https://doi.org/10.1002/cne.902260207>
- Nakamori, H., Naitou, K., Horii, Y., Shimaoka, H., Horii, K., Sakai, H., Yamada, A., Furue, H., Shiina, T., & Shimizu, Y. (2018). Medullary raphe nuclei activate the lumbosacral defecation center through the descending serotonergic pathway to regulate colorectal motility in rats. *American Journal of Physiology—Gastrointestinal and Liver Physiology*, 314(3), G341–G348. <https://doi.org/10.1152/ajpgi.00317.2017>
- Ness, T. J. (2000). Evidence for ascending visceral nociceptive information in the dorsal midline and lateral spinal cord. *Pain*, 87(1), 83–88. [https://doi.org/10.1016/S0304-3959\(00\)00272-4](https://doi.org/10.1016/S0304-3959(00)00272-4)
- Ness, T. J., & Gebhart, G. F. (1987). Characterization of neuronal responses to noxious visceral and somatic stimuli in the medial lumbosacral spinal cord of the rat. *Journal of Neurophysiology*, 57(6), 1867–1892. <https://doi.org/10.1152/jn.1987.57.6.1867>
- Ness, T. J., & Gebhart, G. F. (1988). Characterization of neurons responsive to noxious colorectal distension in the T13–L2 spinal cord of the rat. *Journal of Neurophysiology*, 60(4), 1419–1438. <https://doi.org/10.1152/jn.1988.60.4.1419>
- Ness, T. J., & Gebhart, G. F. (1989). Characterization of superficial T13–L2 dorsal horn neurons encoding for colorectal distension in the rat: Comparison with neurons in deep laminae. *Brain Research*, 486(2), 301–309. [https://doi.org/10.1016/0006-8993\(89\)90516-7](https://doi.org/10.1016/0006-8993(89)90516-7)
- Nishida, K., Matsumura, S., & Kobayashi, T. (2022). Involvement of Brn3a-positive spinal dorsal horn neurons in the transmission of visceral pain in inflammatory bowel disease model mice. *Frontiers in Pain Research*, 3, 979038. <https://doi.org/10.3389/fpain.2022.979038>
- Norgren, R., & Smith, G. P. (1988). Central distribution of subdiaphragmatic vagal branches in the rat. *Journal of Comparative Neurology*, 273(2), 207–223. <https://doi.org/10.1002/cne.902730206>
- Olsson, C., Chen, B. N., Jones, S., Chataway, T. K., Costa, M., & Brookes, S. J. H. (2006). Comparison of extrinsic efferent innervation of guinea pig distal colon and rectum. *Journal of Comparative Neurology*, 496(6), 787–801. <https://doi.org/10.1002/cne.20965>
- Osman, S., Tashtush, A., Reed, D. E., & Lomax, A. E. (2023). Analysis of the spinal and vagal afferent innervation of the mouse colon using neuronal retrograde tracers. *Cell and Tissue Research*, 392(3), 659–670. <https://doi.org/10.1007/s00441-023-03769-3>
- Palecek, J., Paleckova, V., & Willis, W. D. (2003). Fos expression in spinothalamic and postsynaptic dorsal column neurons following noxious visceral and cutaneous stimuli. *Pain*, 104(1–2), 249–257. [https://doi.org/10.1016/S0304-3959\(03\)00013-7](https://doi.org/10.1016/S0304-3959(03)00013-7)
- Palecek, J., & Willis, D. W. (2003). The dorsal column pathway facilitates visceromotor responses to colorectal distention after colon inflammation in rats. *Pain*, 104(3), 501–507. [https://doi.org/10.1016/S0304-3959\(03\)00075-7](https://doi.org/10.1016/S0304-3959(03)00075-7)
- Paxinos, G., & Franklin, K. (2001). *The mouse brain in stereotaxic coordinates* (2nd ed.). Academic Press.
- Polgár, E., Sardella, T. C. P., Tiong, S. Y. X., Locke, S., Watanabe, M., & Todd, A. J. (2013). Functional differences between neurochemically defined populations of inhibitory interneurons in the rat spinal dorsal horn. *Pain*, 154(12), 2606–2615. <https://doi.org/10.1016/j.pain.2013.05.001>
- Qi, L., Lin, S. H., & Ma, Q. (2023). Spinal VGLUT3 lineage neurons drive visceral mechanical allodynia but not sensitized visceromotor reflexes. *Neuron*, 111(5), 669.e5–681.e5.
- Robinson, D. R., Mcnaughton, P. A., Evans, M. L., & Hicks, G. A. (2004). Characterization of the primary spinal afferent innervation of the mouse colon using retrograde labelling. *Neurogastroenterology and Motility*, 16(1), 113–124. <https://doi.org/10.1046/j.1365-2982.2003.00456.x>
- Schneider, C. A., Rasband, W. S., & Eliceiri, K. W. (2012). NIH Image to ImageJ: 25 years of image analysis. *Nature Methods*, 9(7), 671–675. <https://doi.org/10.1038/nmeth.2089>
- Shapiro, R. E., & Miselis, R. R. (1985). The central organization of the vagus nerve innervating the stomach of the rat. *Journal of Comparative Neurology*, 238(4), 473–488. <https://doi.org/10.1002/cne.902380411>
- Smith-Edwards, K. M., Najjar, S. A., Edwards, B. S., Howard, M. J., Albers, K. M., & Davis, B. M. (2019). Extrinsic primary afferent neurons link visceral pain to colon motility through a spinal reflex in mice. *Gastroenterology*, 157(2), 522–536.e2. <https://doi.org/10.1053/j.gastro.2019.04.034>
- Tao, J., Campbell, J. N., Tsai, L. T., Wu, C., Liberles, S. D., & Lowell, B. B. (2021). Highly selective brain-to-gut communication via genetically defined vagus neurons. *Neuron*, 109(13), 2106.e4–2115.e4. <https://doi.org/10.1016/j.neuron.2021.05.004>
- Tokita, K., Inoue, T., & Boughter, J. D. (2009). Afferent connections of the parabrachial nucleus in C57BL/6J mice. *Neuroscience*, 161(2), 475–488. <https://doi.org/10.1016/j.neuroscience.2009.03.046>
- Tomer, R., Ye, L., Hsueh, B., & Deisseroth, K. (2014). Advanced CLARITY for rapid and high-resolution imaging of intact tissues. *Nature Protocols*, 9(7), 1682–1697. <https://doi.org/10.1038/nprot.2014.123>
- Traub, R. J. (2000). Evidence for thoracolumbar spinal cord processing of inflammatory, but not acute colonic pain. *NeuroReport*, 11(10), 2113–2116. <https://doi.org/10.1097/00007156-200007140-00011>
- Traub, R. J., Herdegen, T., & Gebhart, G. F. (1993). Differential expression of c-fos and c-jun in two regions of the rat spinal cord following noxious colorectal distention. *Neuroscience Letters*, 160(2), 121–125. [https://doi.org/10.1016/0304-3940\(93\)90394-Z](https://doi.org/10.1016/0304-3940(93)90394-Z)
- Traub, R. J., & Murphy, A. (2002). Colonic inflammation induces fos expression in the thoracolumbar spinal cord increasing activity in the spinoparabrachial pathway. *Pain*, 95(1–2), 93–102. [https://doi.org/10.1016/S0304-3959\(01\)00381-5](https://doi.org/10.1016/S0304-3959(01)00381-5)
- Traub, R. J., Pechman, P., Iadarola, M. J., & Gebhart, G. F. (1992). Fos-like proteins in the lumbosacral spinal cord following noxious and non-noxious colorectal distention in the rat. *Pain*, 49(3), 393–403. [https://doi.org/10.1016/0304-3959\(92\)90247-9](https://doi.org/10.1016/0304-3959(92)90247-9)

- Travagli, R. A., Hermann, G. E., Browning, K. N., & Rogers, R. C. (2006). Brainstem circuits regulating gastric function. *Annual Review of Physiology*, 68, 279–305. <https://doi.org/10.1146/annurev.physiol.68.040504.094635>
- Wang, F. B., & Powley, T. L. (2000). Topographic inventories of vagal afferents in gastrointestinal muscle. *Journal of Comparative Neurology*, 421(3), 302–324. [https://doi.org/10.1002/\(SICI\)1096-9861\(20000605\)421:3%3c302::AID-CNE2%3e3.0.CO;2-N](https://doi.org/10.1002/(SICI)1096-9861(20000605)421:3%3c302::AID-CNE2%3e3.0.CO;2-N)
- Wang, G., Tang, B., & Traub, R. J. (2005). Differential processing of noxious colonic input by thoracolumbar and lumbosacral dorsal horn neurons in the rat. *Journal of Neurophysiology*, 94, 3788–3794. <https://doi.org/10.1152/jn.00230.2005>
- Wang, L., Martínez, V., Larauche, M., & Taché, Y. (2009). Proximal colon distension induces Fos expression in oxytocin-, vasopressin-, CRF- and catecholamines-containing neurons in rat brain. *Brain Research*, 1247, 79–91. <https://doi.org/10.1016/j.brainres.2008.09.094>
- Werberger, R., & Basbaum, A. I. (2019). Spinal cord projection neurons: A superficial, and also deep analysis. *Current Opinion in Physiology*, 11, 109–115. <https://doi.org/10.1016/j.cophys.2019.10.002>
- Zhang, L. Y., Dong, X., Liu, Z. L., Mo, J. Z., Fang, J. Y., Xiao, S. D., Li, Y., & Chen, S. L. (2011). Luminal serotonin time-dependently modulates vagal afferent driven antinociception in response to colorectal distention in rats. *Neurogastroenterology and Motility*, 23(1), 62–69, e6. <https://doi.org/10.1111/j.1365-2982.2010.01589.x>

How to cite this article: Wang, Q. Q., Carballo, S. G., Rychkov, G., McGovern, A. E., Mazzone, S. B., Brierley, S. M., & Harrington, A. M. (2023). Comparative localization of colorectal sensory afferent central projections in the mouse spinal cord dorsal horn and caudal medulla dorsal vagal complex. *Journal of Comparative Neurology*, 1–32. <https://doi.org/10.1002/cne.25546>